

AD 665430

AB

USAALABS TECHNICAL REPORT 67-14

SUPPRESSION OF TRANSMITTED HARMONIC ROTOR LOADS BY BLADE PITCH CONTROL

By

H. Daughaday

November 1967

**U. S. ARMY AVIATION MATERIEL LABORATORIES
FORT EUSTIS, VIRGINIA**

**CONTRACT DA 44-177-AMC-299(T)
CORNELL AERONAUTICAL LABORATORY, INC.
BUFFALO, NEW YORK**

**This document has been approved
for public release and sale; its
distribution is unlimited.**



**Reproduced by the
CLEARINGHOUSE
for Federal Scientific & Technical
Information Springfield Va 22151**

94



DEPARTMENT OF THE ARMY
U. S. ARMY AVIATION MATERIEL LABORATORIES
FORT EUSTIS, VIRGINIA 23604

This contract was initiated to determine the spanwise and azimuthal variation of blade pitch required to eliminate all vertical

Harmonic airloads
Transmissible (noncanceling) harmonic root shears
Harmonic root shears

It was concluded from the results (an ideal control system had been assumed) that it would be most difficult to design a pitch control system for the elimination of all harmonic airloads, because the radial variations in the required pitch angles changed considerably with azimuth position and because the amplitudes and phases of the required inputs changed considerably with flight condition. Further study of the elimination of all harmonic airloads and of all harmonic root shears is not planned.

The required pitch angle inputs applied solely at the blade root were computed to eliminate the noncanceling oscillatory root shears. Results indicate that, for the UH-1 configuration considered, most of the noncanceling harmonic root shears could be eliminated with second and fourth harmonic blade pitch control. Although the use of a single root pitch mode would be preferable from a simplicity standpoint, the required pitch inputs to eliminate transmitted shears were found to change considerably with flight conditions. This suggests that dual pitch controls with differential pitching motions of inboard and outboard blade sections would be necessary to attain the desired blade angles of attack.

A feasibility study of a rotor system with dual pitch controls is planned. The current program will be extended to include the effects of chordwise blade flexibility, in-plane root shears, and rotor performance.

This report has been reviewed by the U. S. Army Aviation Materiel Laboratories and is considered to be technically sound. It is published for the exchange of information and the stimulation of ideas.

Task 1F125901A14604
Contract DA 44-177-AMC-299(T)
USAAVLABS Technical Report 67-14
November 1967

SUPPRESSION OF TRANSMITTED HARMONIC
ROTOR LOADS BY BLADE PITCH CONTROL

CAL Report BB-2117-S-1

by

H. Daughaday

Prepared by
Cornell Aeronautical Laboratory, Inc.
Buffalo, New York

for

U. S. ARMY AVIATION MATERIEL LABORATORIES
FORT EUSTIS, VIRGINIA

This document has been approved
for public release and sale; its
distribution is unlimited.

SUMMARY

A study is made of the possibility of using higher harmonic pitch angle inputs to eliminate the transmission of oscillatory vertical forces from a helicopter rotor to its driving shaft. The aerodynamic loads that are the source of these objectionable forces are computed by the use of a realistic model which represents the rotor blades by bound vorticity distributions and the wake by a mesh of segmented vortex filaments.

The required pitch angles are first found which will eliminate the oscillatory lift loadings at all radial stations by compensating for the azimuthal variation in the blade tangential velocity and for the nonuniformity of the downwash in the rotor disk. In the computations for this case, an ideal control system is assumed such that continuous radial and azimuthal variations in pitch angle inputs are possible.

In the second part of the study, a method is developed for computing the pitch angle inputs at the blade root required to eliminate the oscillatory root shears at the blade attachment hinge without making the oscillatory lift equal to zero at all radial stations. The inertia forces associated with blade dynamic motions produce root shears which are taken into account in the computations. The computational procedure which is developed is capable of treating either the two-bladed teetering rotor or the three-bladed articulated rotor.

The computed results are based on a two-bladed teetering rotor which is approximately the same as that of the UH-1A configuration except for the assumed differences in pitch control. The required pitch angle inputs are determined for several cases in which different combinations of harmonic root shears are eliminated.

It is found that blade dynamic motions have an important effect on the pitch inputs required. The results indicate that for the configuration considered, most of the oscillatory vertical root shear could be eliminated with blade root pitch inputs at the second and fourth harmonics. Considerable variations in the required pitch inputs are found for different flight conditions.

FOREWORD

The investigation described herein was conducted at the Cornell Aeronautical Laboratory, Inc. (CAL), under U. S. Army Contract DA 44-177-AMC-299(T) during the period June 1965 through July 1966. The program was sponsored by the U. S. Army Aviation Materiel Laboratories (USAAVLABE, Fort Eustis, Virginia, as Task 1F125901A14604 and was administered by Mr. J. H. McGarvey.

Dr. H. Daughaday was the project engineer and author of this report. A large part of the theoretical development was carried out by Mr. T. T. Chang. The contributions of Mr. F. A. DuWaldt to the concepts of Section 2 and the many helpful discussions with Mr. R. A. Piziali in the planning of the computational procedure are appreciated by the author. The programming of the computational procedure for the IBM 7044 EDP was carried out by Mr. R. H. Wahlem.

TABLE OF CONTENTS

	Page
SUMMARY	iii
FOREWORD	v
LIST OF ILLUSTRATIONS	ix
LIST OF TABLES	xi
LIST OF SYMBOLS	xiii
INTRODUCTION	1
1. AERODYNAMICS OF ROTOR-WAKE SYSTEM	6
2. REQUIREMENTS FOR ELIMINATING ALL HARMONIC AIR LOADS	14
DISCUSSION OF SIMPLIFYING ASSUMPTIONS MADE IN ANALYSIS	14
METHOD OF SOLUTION OF INVERSE PROBLEM	18
RESULTS OF COMPUTATIONS FOR PITCH ANGLES REQUIRED TO ELIMINATE ALL HARMONIC AIR LOADS	22
3. METHOD FOR FINDING PITCH ANGLE INPUTS TO ELIMINATE OSCILLATORY ROOT SHEARS	32
DESCRIPTION OF ROTOR DYNAMIC MOTIONS	33
HARMONIC AND DISCRETE TIME TREATMENT OF VARIABLES	35
DISCUSSION OF EQUATIONS OF MOTION AND ANALYTICAL PROBLEM	36
ITERATIVE SCHEME OF SOLUTION FOR HARMONIC MOTIONS AND ROOT SHEARS	44
4. RESULTS OF COMPUTATIONS FOR PITCH ANGLE INPUTS REQUIRED TO ELIMINATE NONCANCELLING OSCILLATORY ROOT SHEARS	48

COMPUTATIONS FOR CONVENTIONAL PITCH CONTROL (WITH AND WITHOUT BLADE TORSION)	48
ELIMINATION OF NONCANCELING ROOT SHEARS FOR FLIGHT CONDITION DN67A (BLADE TORSIONAL DEFLECTIONS ASSUMED ZERO)	50
ELIMINATION OF NONCANCELING ROOT SHEARS. COMPARISON OF REQUIREMENTS FOR FLIGHT CONDITIONS DN66A, DN67A, and DN68A	55
CONVERGENCE DIFFICULTIES IN COMPUTER SOLUTION	60
CONCLUSIONS AND RECOMMENDATIONS	61
REFERENCES	64
APPENDIXES	
I. BLADE PARAMETERS USED IN COMPUTATIONS	66
II. EXPRESSIONS FOR ELEMENTS IN [E], [L], AND [H] MATRICES	70
DISTRIBUTION	77

LIST OF ILLUSTRATIONS

<u>Figure</u>		<u>Page</u>
1	Example of Wake Configuration	6
2	Representation of Blade Section by Chordwise Bound Vorticity Distribution	8
3	Relative Velocities Due to Forward Motion and Blade Rotation (Referred to a Shaft-Oriented Reference System)	13
4	Transverse Velocity of Blade Midchord Axis Relative to Air (Induced Velocities Not Included)	13
5	Blade Segments Used in Computations	16
6	Distribution of Effective Angle of Attack; Normalized to 14 Degrees; UH-1A; $\mu = 0.259$ (Computer Run B-6)	19
7	Computed Lift Loading Distributions for UH-1A at $\mu = 0.259$	21
8	Azimuthal Variations of Blade Pitch Angles Required to Eliminate All Harmonic Air Loads (Modified UH-1A Configuration)	24
9	Radial Variation of Blade Pitch Angles Required to Eliminate All Harmonic Air Loads (Modified UH-1A Configuration)	30
10	Required Mean Pitch Angle Versus Radius Distribution to Eliminate All Harmonic Air Loads	31
11	Schematic Diagram of Modes Used to Describe Motions of a Two-Bladed Teetering Rotor	34
12	Schematic Diagram of the Analytical Problem of Finding Pitch Angle Inputs to Eliminate Oscillatory Root Shears	43
13	Schematic Diagram of Principal Steps in Iterative Solution	47

<u>Figure</u>		<u>Page</u>
14	Comparison of Pitch Control Schedules for Eliminating Noncanceling Harmonic Root Shears. Flight Condition DN67A	53
15	Azimuthal Variation of Noncanceling Root Shears. Flight Condition DN67A	54
16	Effect of Higher Harmonic Pitch Control on Oscillatory Lift Loadings. Flight Condition DN67A. Computer Runs B-10 and B-12	56
17	Effect of Higher Harmonic Pitch Control on Oscillatory Lift Loadings. Flight Condition DN67A. Computer Runs B-8 and B-10	57

LIST OF TABLES

<u>Table</u>		<u>Page</u>
I	Parameters for Adjusted Flight Conditions	23
II	Harmonic Analysis of Geometric Angles of Attack Required to Eliminate Harmonic Air Loads	
(a)	$r/R = 0.400$	26
(b)	$r/R = 0.588$	26
(c)	$r/R = 0.750$	27
(d)	$r/R = 0.850$	27
(e)	$r/R = 0.900$	28
(f)	$r/R = 0.950$	28
(g)	$r/R = 0.987$	29
III	Effect of Blade Torsion on Required Collective and Cyclic Pitch Angles. Flight Condition DN67A with Conventional Control	49
IV	Effect of Blade Torsion on Harmonic Root Shears. Flight Condition DN67A with Conventional Control	49
V	Required Pitch Angles to Eliminate Noncanceling Root Shears. Flight Condition DN67A (No Torsional Deflections)	51
VI	Effect of Higher Harmonic Pitch Angle Inputs on Root Shears. Flight Condition DN67A (No Torsional Deflections)	51
VII	Harmonics and Peak-to-Peak Amplitudes of Bending Moments. Flight Condition DN67A (No Torsional Deflections)	58
VIII	Required Pitch Angles to Eliminate All Noncanceling Root Shears. Comparison of Results for Flight Conditions DN66A, DN67A, and DN68A	59

IX	Natural Blade Frequencies Used in Computations	66
X	Mass, Centrifugal Force, and Stiffness Coefficients for Teetering and Bending Modes	68
XI	Mass, Centrifugal Force, and Stiffness Coefficients for Torsion and Control Modes	69

LIST OF SYMBOLS

A_n	Glauert coefficients
$(A_n q_i), (B_n q_i)$	Fourier coefficients of $q_i(t)$
$A_{\dot{q}\ddot{q}}, A_{\dot{q}_i \dot{q}_j}, A_{q_i q_j}$ $C_{\dot{q}_i \dot{q}_j}, S_{\dot{q}_i \dot{q}_j}, S_{q_i q_j}$	quasi-static aerodynamic coefficients
b	blade semichord
c_l, c_{l_α}	section lift coefficient and lift curve slope
c_i	generalized coordinate for i^{th} control mode
$D(I, J, n)$	dynamic response matrix
e_o	distance of blade pitch axis forward of midchord
e	distance of blade elastic axis forward of midchord
$[E], [L], [H]$	matrices of aerodynamic coefficients used in estimating $\Delta^t[G]$
$f_{q_i}(r)$	normalized deflection in the q_i^{th} mode
$[F]$	response matrix used in iterative solution
G_{q_i}	generalized air load acting in the q_i^{th} mode
\bar{G}_{q_i}	complex periodic variation of G_{q_i}
$g_{q_i q_j}$	structural damping coefficient
$G_{q_i q_j}$	generalized gyroscopic coupling coefficient
h	blade section plunging velocity relative to fixed axes
h	blade deflection relative to reference plane due to preconing and steady blade bending
h_i	generalized coordinate for i^{th} vertical deflection mode
h_m	distance of midchord axis above reference plane
I_k	quasi-steady part of Γ_k

I_x, I_y	moments of inertia about elastic axis due to horizontal and vertical mass distributions, respectively
I, J	indices used to designate rows and columns of matrices
k	subscript denoting collocation points in rotor disk
ℓ	subscript denoting value at azimuth position, $\psi_\ell = 2\pi(\ell-1)/(NA)$
$K_{q_i q_j}$	generalized stiffness coefficient
λ	blade section lift per unit span
m	blade mass per unit span
$M_{q_i q_j}$	generalized mass coefficient
m	blade section pitching moment about midchord per unit span
NA	number of azimuth positions used in the computation
NR	number of blade radial segments used in the computation
NRA	total number of collocation points in rotor disk; $NRA = NR \times NA$
q_i	generalized coordinate for i^{th} vertical deflection, torsional, or control mode
\bar{q}_i	complex periodic variation of q_i
R	total blade radius
r	radius to a blade section
S_c	canceling root shear of one blade
\bar{S}_c	complex periodic variation of S_c
S_n	noncanceling root shear of one blade
\bar{S}_N	complex periodic variation of S_N

S_n	coefficients giving induced velocities due to mesh of vortex filaments in wake
T_n	coefficients giving induced velocities due to rolled-up tip vortices
$T_{q_i q_j}$	generalized centrifugal force coefficient
t	time
t'	dimensionless time; $t' = \omega_c t$
(t)	superscript used to denote t^{th} approximation of iterative solution
v_k	velocity relative to the surface of the airfoil due to plunging motion at the k^{th} collocation position
V_f	rotor translational (forward) velocity
V_r	component of total velocity of blade section perpendicular to the shaft and to the blade axes
W_b	load/blade (lb)
w_k	normal induced velocity distribution at the k^{th} collocation position
x	chordwise coordinate; distance aft of midchord
$[X(n, I)]$	column matrix of n^{th} harmonic Fourier coefficients of root shears and generalized coordinates
$[YP(n, I)]$	column matrix of prescribed variables
$[Y(n, I)]$	column matrix on right hand of equations used in iterative solution for variables
$\bar{Z}_{q_i} = Z_{q_i}$	generalized centrifugal force acting in q_i^{th} mode due to built-in twist and preconing
α_g	geometric angle of attack of blade section relative to V_r
$\dot{\alpha}_g$	time rate of change of geometric angle of attack
α_s	shaft angle relative to plane perpendicular to rotor translational velocity

β	first harmonic flapping relative to a plane perpendicular to the shaft; $\beta = \beta_{1C} \cos \psi + \beta_{1S} \sin \psi$
β_c	preconing angle
Γ_k	total bound vorticity of blade section of k^{th} segment
$\bar{\Gamma}$	strength of rolled-up tip vortex
γ_k	chordwise bound vorticity distribution at the k^{th} collocation position
$\Delta^{(t)}[G]$	change in column matrix of generalized aerodynamic forces from $(t-1)^{\text{th}}$ to $(t)^{\text{th}}$ approximation
θ	angular coordinate used to specify chordwise position; $x = -b \cos \theta$
θ_B	built-in twist
θ_i	generalized coordinate for i^{th} torsion mode
μ	advance ratio
ρ	air density
σ, τ	induced velocity coefficients of Γ -equations
ψ	azimuth angle
Ω	blade rotational speed
ω_{q_i}	natural frequency of q_i^{th} mode
ω_c	characteristic frequency

INTRODUCTION

High fuselage vibration levels are still today a source of passenger discomfort in many helicopters and in some cases are of sufficient magnitude to interfere with the performance of desired helicopter missions. It is generally believed that the primary sources of the objectionable vibrations are the rotor generated forces which are transmitted directly to the shaft and fuselage via the blade root fittings and rotor hub. This report is limited to considering the reduction of forces of this type -- more specifically, the vertically transmitted vibratory root shear forces. It is recognized, however, that it is also necessary to minimize vibration from other sources (e.g., those caused by the engine, transmission, tail rotor, and the aerodynamic excitation of the fuselage by the rotor downwash).

Several different methods of attack have been made on the problem of reducing the vibratory shears which are transmitted directly from the rotor to the fuselage. Passive systems for isolating the rotor head or rotor-engine-transmission system from in-plane vibratory shears have been widely used for many years (e.g., those discussed in Reference 1). Some success has been achieved with this approach in spite of the difficulty of isolating against the large-amplitude, low-frequency vibrations which are characteristic of the helicopter rotor system. Currently, work is being done on various active vibration isolators and force balancing systems (References 2 and 3). However, it will be some time before such systems can be evaluated in service on several different configurations.

Another philosophy of vibration reduction is based on the idea of eliminating the exciting forces in the rotor system rather than isolating them from the rest of the helicopter. This concept is well accepted as regards the elimination of mechanical unbalance or forces caused by dissymmetry between blades. Attempts have also been made to reduce the amplification of the response in the natural bending modes of blades by the addition of appropriate ballast weight to shift the natural bending frequencies and/or increase the effective aerodynamic damping (Reference 4). Reductions in bending vibrations obtained in this manner would, at the same time, reduce the associated root shears transmitted to the shaft. Another approach has involved the application of second harmonic pitch control both to reduce vibration exciting forces and to obtain certain performance benefits (Reference 5).

In this report, further consideration is given to the possibility of reducing vertical rotor shaking forces by the application of suitable blade pitch angle control. The work reported, which has been largely exploratory, started with finding the requirements for eliminating all aerodynamic exciting forces with an assumed ideal control system

such that continuous radial and azimuthal variations in pitch angle inputs would be possible. However, emphasis has been placed on studying some of the inherent dynamic problems in eliminating root shears with pitch inputs applied solely at the blade root. The study has been limited to the application of pitch control for the reduction of vibrations, and the effect of such pitch changes on aerodynamic performance remains to be determined. Such an evaluation should, of course, include an estimate of the weight and power requirements of the controlling mechanism.

In this first study of the problem, it was decided to consider only lift or vertical shear loads transmitted to the fuselage. It is well known that vibratory drag loads generated in the rotor system are also responsible for serious fuselage vibrations, and further work is required to determine if they too can be reduced by blade pitch control.

The vibratory aerodynamic forces acting on a rotor blade are dependent upon the induced velocities produced by the vorticity in the wake of the rotor. Careful consideration of the effect of the wake vorticity is necessary if a realistic estimate is to be made of the blade pitch angles required to eliminate vibratory blade loads and root shears. A summary is given in Section 1 of the method of treatment which has been used for the aerodynamics of the rotor-wake system.

The objective of the investigation was to determine the spanwise and azimuthal distribution of blade geometric angles of attack required to eliminate:

- A. All harmonic air loads.
- B. All transmissible (noncanceling) harmonic root shears.
- C. All harmonic root shears.

The requirements for eliminating all harmonic air loads (Case A) are taken up in Section 2. The purpose of the study discussed in this section is to find the radial and azimuthal variations in blade pitch angles required to obtain a blade lift loading which does not vary with azimuth position and thus is optimum from the standpoint of avoiding oscillatory root shears and blade vibrations.

However, the elimination of all noncanceling harmonic root shears (Case B) can be accomplished without imposing the severe requirement of an azimuthally independent blade load distribution. It is only necessary that the integral of the harmonic lift and inertia force loadings over the entire rotor be zero; the blade pitch input requirements are made easier for this case by the fact that the root shears of the separate blades cancel at some harmonics. In the event of dissymmetry between blades preventing perfect cancellations, all transmitted

loads could be eliminated by requiring that all harmonic root shears be zero for each blade individually (Case C). It would be expected that consideration of Case C would not be necessary for a helicopter rotor built with reasonable manufacturing tolerances.

The radial variations of pitch angles required to make the harmonic root shears zero are not unique. A computational procedure is formulated in Section 3 for treating Cases B and C which assumes that pitch angle inputs are introduced by one or two control modes at each harmonic.

A successive approximation solution is indicated in Section 3 for obtaining blade loads, blade motions, and required pitch control inputs. The current approximations for the blade air loads, computed by the procedure of Section 1, are used as inputs for dynamic response computations which give new blade motions to be used in the computations for the next approximation for the air loads. The procedure provides for including flapwise and torsional blade dynamics but neglects in-plane dynamic motions.

In order to aid convergence of the overall solution, the blade air loads, which are computed from the current approximation for the blade motions, are not used directly in the response computations for the next approximation but are, in effect, combined with incremental air loads based on estimates of the change in air loads from the current to the next approximation. The increments in air loads from one iteration to the next become smaller and smaller as the solution converges, so that the final solution does not depend on the method used for estimating the incremental air loads.

It was hoped that satisfactory convergence of the solution could be obtained using estimated incremental air loads based on quasi-static aerodynamic coefficients which could be precomputed before the solution of the main problem. However, it was found that the incremental air loads based on quasi-static theory were not sufficiently accurate for all cases.

In general, convergence difficulties were encountered when the torsional degrees of freedom were included in the computations. For example, a torsional mode near resonance caused convergence difficulties in computations carried out for the reference case of conventional helicopter control using zero-harmonic collective and first-harmonic cyclic pitch inputs. The computer solution for this case did not converge when the estimated incremental air loads for this torsion mode were based on quasi-static aerodynamic theory. However, satisfactory convergence was obtained when an improved estimate of the incremental torsional air loads was used which was based on coefficients derived from the change in loads from one

iteration to the next in the nonconvergent solution. These same coefficients were tried in a solution for Case B, but convergence difficulties were again encountered when the torsional degrees of freedom were included. It appeared that further refinement of the prediction of the incremental torsional air loads would be necessary in treating Cases B and C, but this could not be attempted within the limits of the research program.

Solutions for Case B which were obtained by assuming that the torsional deflections were zero are discussed in Section 4. The requirements for eliminating only the second- and fourth-harmonic noncanceling shears are considered as well as those for the elimination of all noncanceling root shears. A comparison of these results indicates some of the problems introduced by blade flapwise dynamics in eliminating oscillatory root shears by pitch control.

No computational results are presented for the pitch inputs required to eliminate all harmonic root shears for each blade individually (Case C). Convergence difficulties were encountered for this case even when the torsional deflections were set equal to zero. Methods for improving the estimated incremental air load in order to obtain convergence were not studied for this case.

In making numerical computations, a specific configuration has been assumed. Also, several assumptions have been made to simplify the computations which were not essential to the methods developed. Furthermore, criteria other than the elimination of oscillatory vertical lift load and root shears have not been used in finding the required higher harmonic blade pitch inputs. In order to clarify the basis for the numerical results, the principal assumptions and limitations made in obtaining them are summarized below:

1. The blade feathering and torsional elastic axes are assumed to be coincident at the quarterchord and to intersect with the shaft axis.
2. A preconing angle of 3.0 degrees is assumed.
3. The blade is assumed to be mass balanced about the elastic axis.
4. Compressibility effects are not considered.
5. The wake vorticity is represented by a mesh of vortex filaments.
6. The chordwise vorticity distribution at a given radial station is represented by a Glauert series.

7. Three-dimensional aerodynamic effects are introduced by satisfying normal flow boundary conditions at each radial station including the induced velocities due to wake vorticity.
8. In-plane root shears, flexibility, and deflections are not considered.
9. Rotor performance and aircraft flying qualities are not considered in finding required pitch angles.

Additional special assumptions which are applicable to Sections 2 and 3 are listed at the beginning of those sections.

1. AERODYNAMICS OF ROTOR-WAKE SYSTEM

The treatment of the aerodynamics of the rotor-wake system is basically the same as that used in Reference 6. Consequently, only an abbreviated description of the aerodynamic analysis is given here, and the reader is referred to the cited reference for further details and a justification of the wake model used.

The shed and trailing vorticity distributions in the wake of each blade are represented by an arrangement of straight-line vortex filaments as indicated in Figure 1. For simplicity, the case of only

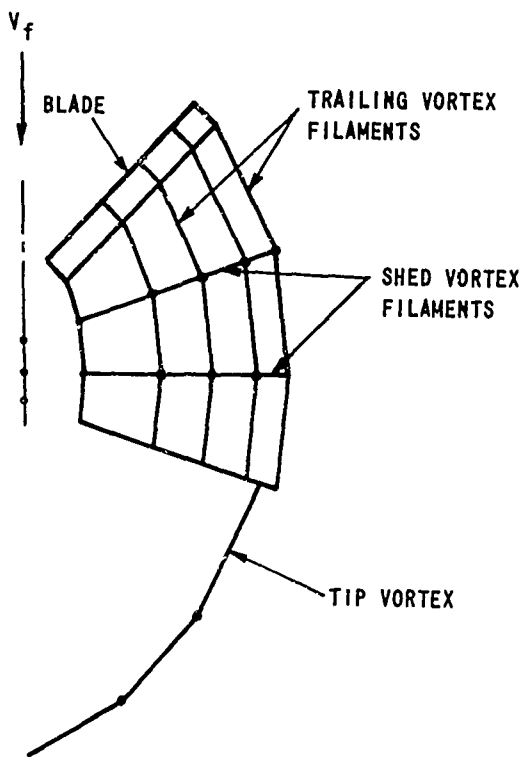


Figure 1 EXAMPLE OF WAKE CONFIGURATION

four radial blade segments is shown on the diagram i.e., $NR = 4$. Trailing vortex filaments arise only at the ends of the blade segments, since it is assumed that there is no radial variation in bound vorticity along each segment. Shed vorticity is deposited continuously in the wake behind each blade of an actual rotor with an intensity equal to the rate of change of bound vorticity. However, the numerical solution is carried out discontinuously using discrete time or azimuth angle increments. The discontinuous azimuth angles are denoted by ψ with a small script letter used as a subscript (e.g., ψ_k or ψ_l). The equally spaced azimuth angles are given by the formula $\psi_k = 2\pi(k-1)/(NA)$, where k takes on all integer values from one to the total number of azimuth positions (NA). The shed vorticity deposited by each blade segment in a given time increment is lumped into a single shed vortex filament in the computational model as indicated on the sketch. This concentrated vortex filament is shed from the trailing edge at the position corresponding to 70 percent of the time increment. Results in Reference 6 show that this procedure gives a reasonable approximation of the shed wake.

The grid of straight-line vortex filaments representing the shed and trailing vortex filaments can be truncated after a prescribed number of azimuth increments. Further aft, the wake is continued as a tip trailing vortex filament representing the rolled-up vortex sheet. Although the computational program permits the use of a distorted wake, the motions of the end points of each wake segment were computed using uniform inflow theory.

In carrying out the solution, boundary conditions are satisfied for NA equally spaced azimuth positions of the rotor at the midpoints of the NR spanwise segments of a given blade. The total bound vorticity or circulation around the airfoil for each of these ($NR \times NA = NRA$) blade segment collocation positions is denoted by Γ with a lower case letter as a subscript (e.g., Γ_j or Γ_k). The integer subscripts j or k are used to specify successive blade segment collocation positions for the entire rotor disk running from the inboard to the outboard segments at the aft azimuth position and then to the inboard segment at the next azimuth position, etc.

For a periodic problem, the strength of each trailing or shed vortex filament can be expressed by a linear combination of the Γ 's in the rotor disk as a consequence of the vorticity conservation laws. When the bound vorticity strengths in adjacent blade segments are Γ_j and Γ_{j+1} , the strength of the trailing vortex segment arising at their intersection must be $\Gamma_j - \Gamma_{j+1}$. The strength of the shed vortex filament immediately aft of a given blade segment is equal to the difference of the bound vorticities of the blade segment at the preceding and current azimuth positions. Similar considerations can be used to find the strengths of all the vortex filaments in a wake representation such as shown in Figure 1.

The strength of the trailing vortex segment produced by the rolling up of the vorticity deposited in the wake between azimuth positions ψ_{k-1} and ψ_k is denoted by $\bar{\Gamma}_k$. It is assumed that $\bar{\Gamma}_k$ is equal in magnitude to the largest of the bound vorticities (Γ_j 's) at azimuth position ψ_k . This amounts to assuming that all the trailing vorticity deposited in the wake outboard of the radial position of maximum bound vorticity is concentrated in the tip vortex.

Each segment of the blade at each discrete azimuth position is represented by a continuous distribution of vorticity aligned in the radial direction and varying in intensity only in the chordwise direction. Using the notation of Reference 6 as indicated in Figure 2, the bound vorticity of a blade segment at collocation position (k) can be expressed by the Glauert series,

$$\gamma_k(\theta) = 2 \left[A_{0k} \cot \frac{\theta}{2} + \sum_{n=1}^{\infty} A_{nk} \sin n\theta \right] \quad (1)$$

where

$$x = -b \cos \theta. \quad (2)$$

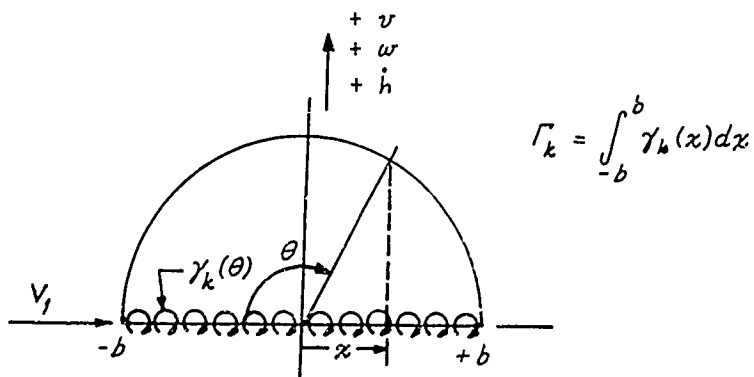


Figure 2 REPRESENTATION OF BLADE SECTION BY CHORDWISE BOUND VORTICITY DISTRIBUTION

The condition for no normal flow through the blade chord at the midspan of a particular blade segment can be expressed as follows:

$$v_k(x) + \omega_k(x) - \frac{1}{2\pi} \int_{-b}^b \frac{\gamma_k(\xi) d\xi}{x - \xi} = 0, \quad (3)$$

where

$$v_k(x) = (-\dot{h} + V, \alpha_{g_k} + \dot{\alpha}_{g_k} x)_k \quad (4)$$

and

$$\omega_k(x) = \sum_{j=1}^{NRA} C_{k_j}(x) \bar{l}_j. \quad (5)$$

The symbol v_k denotes the velocity relative to the surface of the airfoil due to plunging motion (\dot{h}_k) and geometric angle of attack (α_{g_k}) while ω_k is the normal velocity induced by the trailing and shed vortex filaments in the wake. It is noted that the expression for ω_k can be written in terms of the bound vorticity strengths because the strength of each wake vortex segment is a function of the \bar{l}_j 's. The integral in Equation (3) gives the induced velocity due to the bound vorticity. An approximation for this induced velocity is used which should be reasonable at the midspan of the k^{th} blade segment; it is based on the assumption that the bound vorticity representing the k^{th} blade segment is extended to infinity in both directions. This explains the use of the two-dimensional Biot-Savart law in the integral term.

It is convenient to replace the chordwise variable x in Equations (3), (4), and (5) by the expression defined in Equation (2). Then, the evaluation of the integral in Equation (3) gives the well-known result,

$$\begin{aligned} \frac{1}{2\pi} \int_{-b}^b \frac{\gamma_k(\xi) d\xi}{x - \xi} &= \frac{-1}{2\pi} \int_0^\pi \frac{\gamma_k(\phi) \sin \phi d\phi}{(\cos \theta - \cos \phi)} \\ &= A_{o_k} - \sum_{n=1}^{\infty} A_{n_k} \cos n\theta, \end{aligned} \quad (6)$$

where the series in Equation (1) has been substituted for $\gamma_k(\phi)$ replacing θ by ϕ . It is also possible to expand ω_k in a cosine series which is written in the form,

$$\omega_k(\theta) = \sum_{j=1}^{NRA} \left(S_{o_{k_j}} + \sum_{n=1}^{\infty} S_{n_{k_j}} \cos n\theta \right) \bar{l}_j + \sum_{\ell=1}^{NA} \left(T_{o_{k_\ell}} + \sum_{n=1}^{\infty} T_{n_{k_\ell}} \cos n\theta \right) \bar{l}_\ell. \quad (7)$$

The following set of equations results from substituting Equations (4), (6), and (7) into Equation (3), and from requiring that the coefficients of each harmonic cosine term be zero separately:

$$\left. \begin{aligned} A_{0k} &= (-\dot{h} + V_1 \alpha_g)_k + \sum_{j=1}^{NRA} S_{0k_j} \Gamma_j + \sum_{\ell=1}^{NA} T_{0k_\ell} \bar{\Gamma}_\ell, \\ A_{1k} &= (+b \dot{\alpha}_g)_k - \sum_{j=1}^{NRA} S_{1k_j} \Gamma_j - \sum_{\ell=1}^{NA} T_{1k_\ell} \bar{\Gamma}_\ell, \\ A_{nk} &= -\sum_{j=1}^{NRA} S_{nk_j} \Gamma_j - \sum_{\ell=1}^{NA} T_{nk_\ell} \bar{\Gamma}_\ell; \quad n = 2, 3, 4. \end{aligned} \right\} \quad (8)$$

A relationship between the Γ 's and A 's is required before a solution can be found. This is obtained by integrating the Glauert series for the bound vorticity over the chord giving the following expression for the total bound vorticity or circulation about blade segment k ,

$$\begin{aligned} \Gamma_k &= b \int_0^\pi \gamma_k(\theta) \sin \theta d\theta \\ &= 2\pi b \left(A_0 + \frac{1}{2} A_1 \right)_k. \end{aligned} \quad (9)$$

Since the theoretical circulation and the theoretical lift curve slope are not achieved in practice, an empirical correction of Equation (9) is made by multiplying by $c_{L\alpha}/2\pi$, giving

$$\Gamma_k = (c_{L\alpha})_k b_k \left(A_0 + \frac{1}{2} A_1 \right)_k. \quad (10)$$

The result of combining Equations (10) and (8) is

$$\Gamma_k = I_k + \sum_{j=1}^{NRA} \sigma_{kj} \Gamma_j + \sum_{\ell=1}^{NA} \tau_{k\ell} \bar{\Gamma}_\ell, \quad (11)$$

where

$$I_k = (c_{\ell\alpha})_k b_k \left(-\dot{h} + V_r \alpha_g + \frac{1}{2} b \dot{\alpha}_g \right)_k , \quad (12)$$

$$\sigma_{kj} = (c_{\ell\alpha})_k b_k \left(S_{okj} - \frac{1}{2} S_{ikj} \right) , \quad (13)$$

and

$$\tau_{kj} = (c_{\ell\alpha})_k b_k \left(T_{okj} - \frac{1}{2} T_{ikj} \right) . \quad (14)$$

Equation (11) represents a set of (*NRA*) equations which are solved iteratively for the *NRA* β_j 's by the Gauss-Sidel method. In each iteration, the β_j 's for the different spanwise blade segments at a given azimuth angle (ψ_k) must be compared to find their maximum value $\bar{\beta}_k$.

The treatment of stalled and reversed flow regions which is used in Sections 3 and 4 is carried out in the manner described in Reference 6. It is assumed that stall limits the maximum value of β_j attainable at each blade segment collocation position, and this maximum value is introduced as an additional constraint in the iterative solution.

Once the set of equations for the β_j 's (i.e., Equation (11)) has been solved, the strengths of the bound vortices of the blade segments are known for all collocation positions in the rotor disk. Equation (8) can be used to compute the corresponding coefficients (A_{nk} 's) of the Glauert expansions of the chordwise vorticity distributions at these positions. The time derivatives of the Glauert coefficients for a given blade segment are also required in the computations. They are determined by assuming that all variables change periodically at steady flight conditions. This assumption makes it possible to express the time derivatives of the Glauert coefficients for a given blade segment at a particular azimuth position in terms of the values of the Glauert coefficients for the blade segment at all of the *N* equally spaced azimuth positions which are used in the computations.

The linearized Bernoulli equation for unsteady flow leads to an expression for the chordwise variation in pressure difference on a blade segment as it moves through collocation position (k) in terms of the Glauert coefficients and time rate of change of the Glauert coefficients for the blade segment at position (k). This pressure distribution is used to compute the lift and pitching moment per unit span as a function of the values and time derivatives of the Glauert coefficients of a blade segment at position (k). An empirical correction factor is also introduced in

these expressions to allow for the fact that the actual circulation is less than the theoretical value. The expressions for lift and pitching moment (about the midchord) per unit span of a blade segment at collocation position (k) can then be written in the form,

$$l_k = \left\{ c_{l_\alpha} b \rho V_1 \left(A_0 + \frac{1}{2} A_1 \right) + \pi b^2 \rho \frac{\partial}{\partial t} \left(3A_c + A_1 + \frac{1}{2} A_2 \right) \right\}_k \quad (15)$$

$$m_k = \left\{ \frac{1}{2} c_{l_\alpha} b^2 \rho V_1 \left(A_0 + \frac{1}{2} A_1 \right) + \frac{1}{2} \pi b^2 \rho V_1 (-A_1 + A_2) - \frac{1}{2} \pi b^3 \rho \frac{\partial}{\partial t} \left(A_0 + \frac{3}{4} A_1 - \frac{1}{4} A_3 \right) \right\}_k \quad (16)$$

The lift and moment loadings obtained from Equations (15) and (16) are those resulting from the given geometric angles of attack (α_{g_k}), rates of change of geometric angle of attack ($\dot{\alpha}_{g_k}$), and plunging velocities (\dot{h}_k) entering in Equations (8) and (12). These quantities must be defined in terms of the geometry and motion of the rotor system.

The shaft-oriented reference system used in the analysis is shown in Figure 3 and the deflected blade axis is indicated schematically in Figure 4. The following expressions for the velocity components used in the analysis are readily derived by reference to these figures.

$$V_r = \Omega r + (V_f \cos \alpha_s) \sin \psi \quad (17)$$

= component of relative velocity perpendicular to the shaft and to the blade axis.

$$\dot{h} = V_f \sin \alpha_s \cos \left(\frac{dh_m}{dr} \right) + V_f \cos \alpha_s \cos \psi \sin \left(\frac{dh_m}{dr} \right) + \dot{h}_m \cos \left(\frac{dh_m}{dr} \right)$$

= component of velocity perpendicular to V_r and the blade axis (i. e., velocity of airfoil relative to air excluding induced velocity).

By making use of small angle approximations,

$$\dot{h} = V_f \sin \alpha_s + V_f \cos \alpha_s \cos \psi \frac{dh_m}{dr} + \dot{h}_m. \quad (18)$$

Forward velocity is denoted by V_f , shaft angle by α_s , and the distance of the midchord axis above the reference plane by h_m .

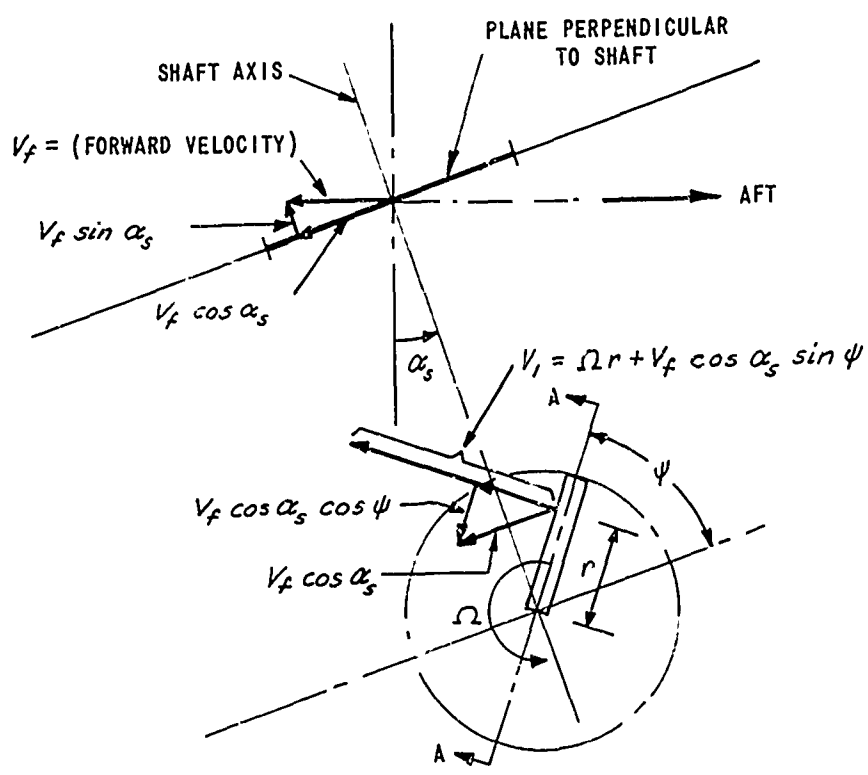


Figure 3 RELATIVE VELOCITIES DUE TO FORWARD MOTION AND BLADE ROTATION (REFERRED TO A SHAFT-ORIENTED REFERENCE SYSTEM)

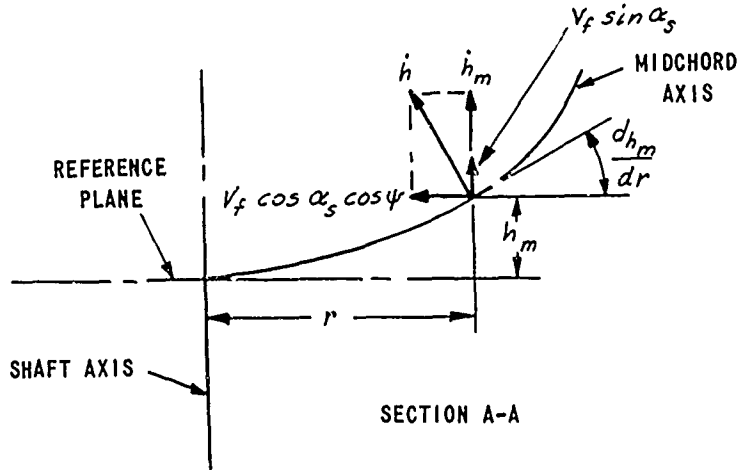


Figure 4 TRANSVERSE VELOCITY OF BLADE MIDCHORD AXIS
RELATIVE TO AIR (INDUCED VELOCITIES NOT INCLUDED)

2. REQUIREMENTS FOR ELIMINATING ALL HARMONIC AIR LOADS

This section takes up the requirements on the spanwise and azimuthal variations of blade geometric angles of attack which are necessary to eliminate all harmonic lift loads on helicopter rotors (Case A), and thus to obtain a spanwise lift distribution which does not vary with azimuth position. The elimination of all harmonic loads will be defined as the elimination of all oscillatory lift loads through the twelfth harmonic. The following special assumptions are made in this section in developing a method for finding the required pitch angles:

1. The harmonic lift loads at all spanwise stations are assumed to be zero for the first through the twelfth harmonic.
2. The rotor blade is assumed to be modified such as to preclude the reversed flow region.
3. Simplifications are made in the Section I treatment of rotor aerodynamics on the basis of assuming the reduced frequencies to be small at all harmonics of importance.

It is not anticipated that the pitch change schedule which is required for obtaining the desired load distribution could be implemented exactly with an actual helicopter. However, study of this ideal case is useful for seeing the possibilities and limitations of practical systems.

In the usual method for the computation of blade loads, including the effect of wake vorticity, the lift is determined for given blade pitch angle changes. This procedure might be iterated several times with the objective of finding the required pitch angles to eliminate all harmonic air loads. Instead, the inverse problem is considered which consists of solving directly for the geometric blade angles necessary to produce a constant specified lift distribution. Simplifying assumptions 2 and 3, which are given above, are made in order to make practicable the solution of the inverse problem. These approximations are believed to be sufficiently accurate for a general study of the problem.

DISCUSSION OF SIMPLIFYING ASSUMPTIONS MADE IN ANALYSIS

In order to eliminate nonlinearities associated with reverse flow, the innermost blade airfoil section is assumed to be sufficiently far outboard to eliminate the reverse flow region completely; any aerodynamic forces on the root attachment fitting are neglected.

A comparison is made in Figure 5 of the standard UH-1A blade plan-form used in the computations of Section 4 and the modified blade on which the computational results of this section are based. The blade feathering and elastic axes are assumed to be coincident at the quarter-chord as shown in Figure 5c.

Since the aerodynamic lift distribution for Case A is assumed to be constant as the rotor turns, there will be no aerodynamic forces tending to excite oscillatory teetering or bending motions of the blades relative to the rotor disk. If, in addition, the blade is assumed to be dynamically balanced, there is no need for considering blade bending dynamics in the analysis.

The computations for the required spanwise and azimuthal variations in blade geometric angles of attack give the sum of the pitch control and torsional deflections at each radial station. Since no control system is being postulated here, it is immaterial how the total blade angle is divided between pitching and torsional motions. Torsional dynamics are not included in the analysis because calculations are not performed to separate the total angles into torsional deformations and control inputs. Meaningful computations for torsional deformations cannot be made without specifying a control input mechanism.

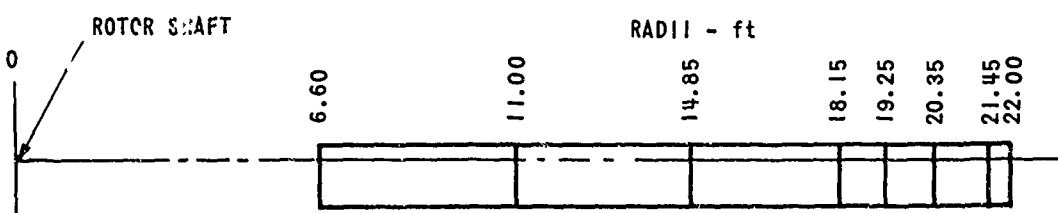
In order to indicate other simplifying assumptions which are made, it is convenient to introduce the dimensionless time,

$$t' = \omega_c t$$

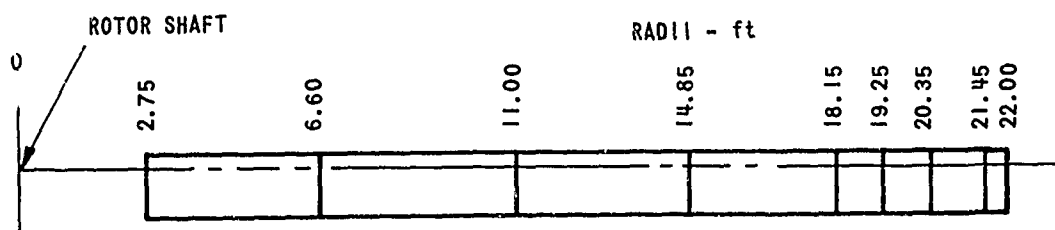
and rewrite Equations (10), (11), and (15) in the form

$$\Gamma_k = c_{\alpha} \varepsilon_k b_k \left(A_0 + \frac{1}{2} A_1 \right)_k , \quad (19)$$

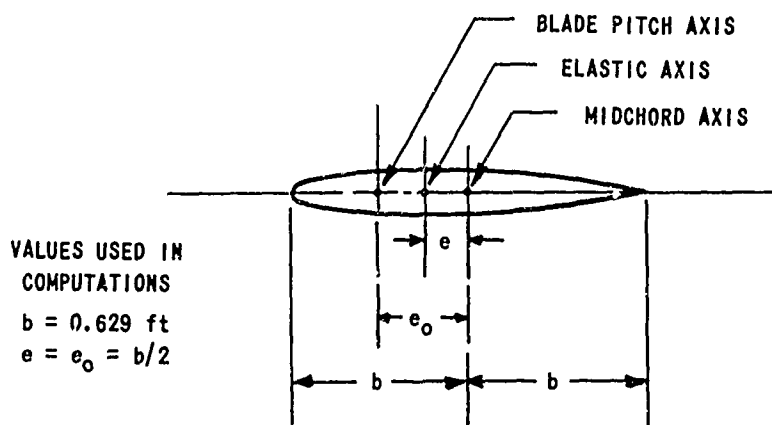
$$\begin{aligned} \Gamma_k &= (c_{\ell\alpha})_k b_k V_{t_k} \left[-\left(\frac{b\omega_c}{V_1}\right)\left(\frac{r}{b}\right) \frac{\partial\left(\frac{h}{r}\right)}{\partial t'} + \alpha_g + \frac{1}{2} \left(\frac{b\omega_c}{V_1}\right) \frac{\partial\alpha_g}{\partial t'} \right]_k \\ &\quad + \sum_{j=1}^{NRA} \sigma_{k_j} \Gamma_j + \sum_{\ell=1}^{NA} \tau_{k_\ell} \bar{\Gamma}_\ell . \end{aligned} \quad (20)$$



a. MODIFIED UH-1A BLADE PLANFORM
(USED IN COMPUTATIONS OF SECTION 2)



b. UH-1A BLADE PLANFORM
(USED IN COMPUTATIONS OF SECTION 4)



c. ASSUMED LOCATION OF BLADE PITCHING AND ELASTIC AXES

Figure 5 BLADE SEGMENTS USED IN COMPUTATIONS

and

$$\ell_k = 2\pi\rho b_k V_{1k} \left\{ \frac{c_{\ell\alpha}}{2\pi} \left(A_0 + \frac{1}{2} A_1 \right) + \frac{1}{2} \left(\frac{b\omega_c}{V_1} \right) \frac{\partial}{\partial t'} \left(3A_0 + A_1 + \frac{1}{2} A_2 \right) \right\}_k . \quad (21)$$

The magnitude of the characteristic frequency ω_c is to be selected such that the derivatives of the variables with respect to dimensionless time, t' , are of the same order or smaller than the original variables. It is clear that the characteristic frequency will be of the order of the highest harmonics of importance in a Fourier series description of the loading. The simplifying assumption is made that

$$\frac{b\omega_c}{V_1} \ll 1 , \quad (22)$$

which is equivalent to assuming that the reduced frequencies at all harmonics of importance are small. On the basis of the assumption in Equation (22), the $\partial\alpha_g/\partial t'$ term in Equation (20) and the time derivative term in Equation (21) are dropped. In Equation (20), the dimensionless linear deflection (h/r) is of the order of the variable part of α_g in the outer part of the blade. On the other hand, the ratio of the radial position to the semichord, (r/b), becomes a large number near the blade tip. Thus, it appears that the $(\partial/\partial t')(h/r)$ term in Equation (20) may be of larger magnitude than the other time derivative term and is retained. When the approximations indicated above are made and Equation (19) is substituted into Equation (21), the following simplified equations result which are the basis for the analysis in this section:

$$r'_k = c_{\ell\alpha_k} b_k (V_1 \alpha_g - h)_k + \sum_{j=1}^{NRA} \sigma_{kj} r'_j + \sum_{\lambda=1}^{NA} \tau_{k\lambda} \bar{r}'_\lambda \quad (23)$$

$$\ell_k = (\rho V_1 r')_k . \quad (24)$$

Equation (18) is used to evaluate $\dot{h} = \partial h / \partial t$ setting

$$\frac{dh_m}{dr} = \beta + \frac{dh_o}{dr},$$

$$\dot{h}_m = r\dot{\beta} - \frac{b}{2} \dot{\alpha}_g \approx r\dot{\beta},$$

and

$$\beta = \beta_{1c} \cos \psi + \beta_{1s} \sin \psi,$$

where β is the first harmonic flapping relative to a plane perpendicular to the shaft and h_o is the deflection due to preconing and steady blade bending. The $\dot{\alpha}_g$ term in \dot{h}_m is dropped in accordance with the assumptions made in simplifying Equation (20). After substituting the above relations into Equation (18), the following expression for \dot{h} results:

$$\begin{aligned} \dot{h} = & V_f \sin \alpha_s + V_f \cos \alpha_s \cos \psi \left(\frac{dh_o}{dr} + \beta_{1c} \cos \psi + \beta_{1s} \sin \psi \right) \\ & + (-r\Omega \beta_{1c} \sin \psi + r\Omega \beta_{1s} \cos \psi). \end{aligned} \quad (25)$$

METHOD OF SOLUTION OF INVERSE PROBLEM

As mentioned previously, a constant lift distribution along the blade is specified in the solution of the "inverse blade loading problem". A number of possible criteria might be considered in specifying the loading distribution (e.g., one to obtain maximum lift, minimum power, etc.). In the present program, it was desired that computations be carried out for typical rotor operating conditions for which data were available. The conditions selected for analysis were approximately the same as those obtained in flight test conditions DN66, DN67, and DN68 of Reference 7 which were at advance ratios of $\mu = 0.215, 0.259$ and 0.251 , respectively.

Figure 6 presents the distribution of effective angle of attack of the standard UH-1A configuration at $\mu = 0.259$ as obtained by computations discussed in Section 4. The reverse-flow region is crosshatched while the boundary of the stall region is shown with a dashed line. The assumptions for eliminating the reverse-flow region have already been discussed. Elimination of the stall region can be accomplished by decreasing the effective angle of attack in the inboard portion of the span but compensating increases must be made in the effective angles of attack near the blade tip if the total thrust is to be unchanged. It was

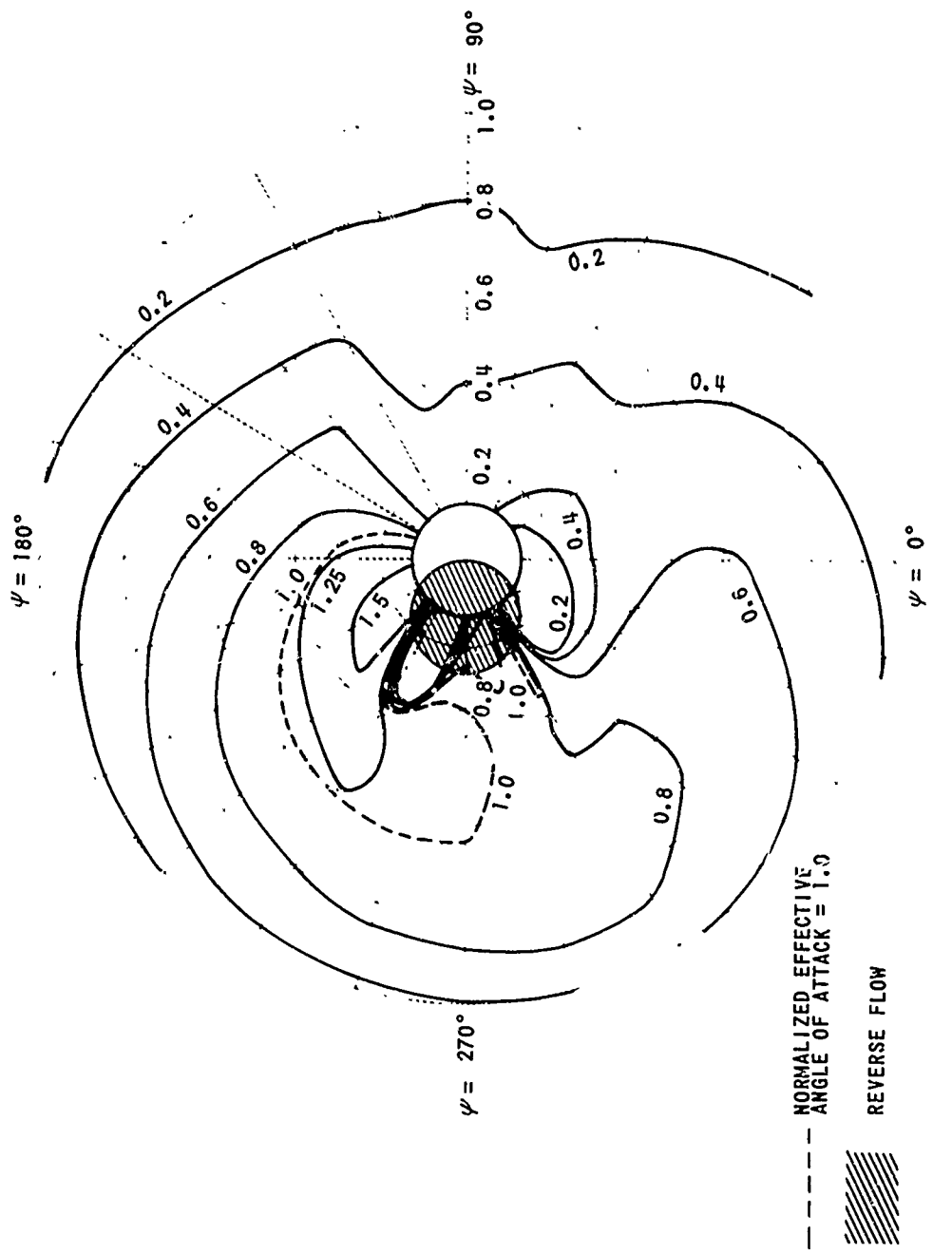


Figure 6 DISTRIBUTION OF EFFECTIVE ANGLE OF ATTACK;
NORMALIZED TO 14 DEGREES; UH-1A; $\mu = 0.259$
(COMPUTER RUN B-6)

found that, in order to obtain the thrust corresponding to the $\mu = 0.259$ condition with an azimuthally independent load distribution, the retreating blade would have to be operating close to stall at all radial positions.

Therefore, it is assumed that the specified lift distribution is the one obtained at azimuth angle $\psi = 270$ degrees with c_L constant along the span;

$$l = c_L \frac{1}{2} \rho (2b) (V_1)^2_{\psi=270} \quad (26)$$

$$= c_L \frac{1}{2} \rho (2b) (\Omega r - V_f \cos \alpha_s)^2. \quad (27)$$

In Figure 7, the lift distribution given by Equation (27) is compared with the computed lift of the standard UH-1A blade at an advance ratio of $\mu = 0.259$. The magnitude of c_L in Equation (27) is selected such that the integrated lift loading gives the desired total lift per blade. As mentioned previously, the c_L required for the $\mu = 0.259$ flight condition results in the blade's being close to stall at $\psi = 270$ degrees. More freedom in rotor design would be desirable, making it possible to obtain the same total lift while operating at lower section lift coefficients. This might be accomplished by a proper compromise of blade taper and changes in average chord and blade radius. If the blade design were revised in this manner, it might also be possible to choose a specified lift distribution with a lower tip loading in order to reduce compressibility effects on the advancing blade. Compressibility effects have not been considered in this work,

The lift loading specified by Equation (27) is to be maintained constant at all azimuth positions and when equated to Equation (24) gives the following expression for the bound vorticity strength at an arbitrary blade segment position k :

$$\Gamma_k = c_L b_k (\Omega r_k - V_f \cos \alpha_s)^{\frac{1}{2}} / V_{t_k}. \quad (28)$$

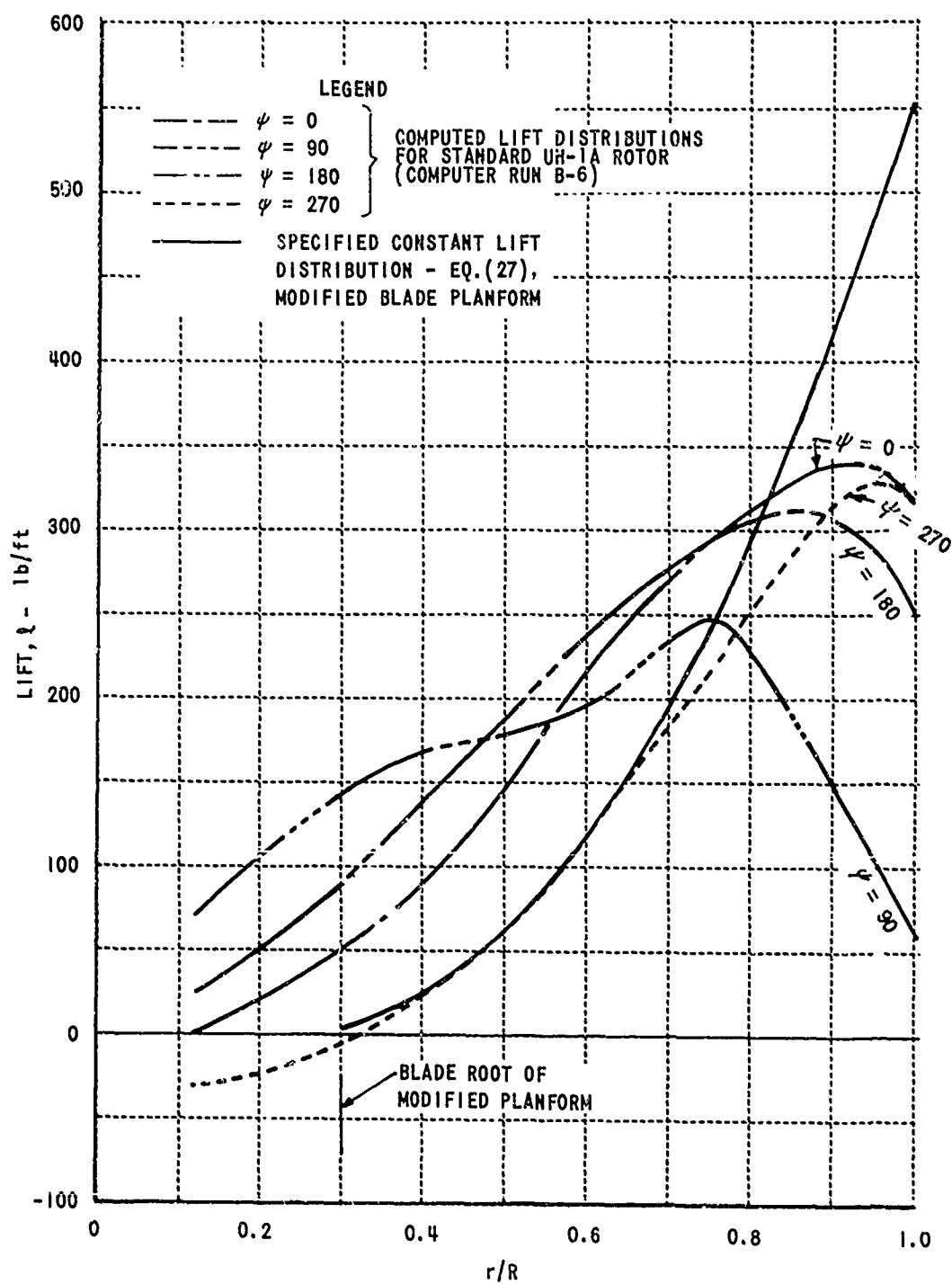


Figure 7 COMPUTED LIFT LOADING DISTRIBUTIONS FOR UH-1A AT $\mu = 0.259$

Having found the bound r_j 's for all radial and azimuth positions by Equation (28), the geometric angles of attack required to obtain the prescribed loading can be computed from Equation (23) rearranged as follows:

$$\alpha_{gk} = \frac{1}{(c_{\ell\alpha})_k b_k V_{f_k}} \left\{ r_k - \sum_{j=1}^{NRA} \sigma_{kj} r_j + \sum_{\ell=1}^{NA} \tau_{k\ell} \bar{r}_\ell \right\} + \frac{1}{V_{f_k}} (h_k). \quad (29)$$

The h_k term is computed from Equation (25) for a prescribed tip-path-plane position and the average deflection due to the prescribed loading.

RESULTS OF COMPUTATIONS FOR PITCH ANGLES REQUIRED TO ELIMINATE ALL HARMONIC AIR LOADS

Computations were carried out for three different flight conditions using the parameters shown in Table I. These conditions are approximately the same as those that existed in flight test conditions DN66, DN67, and DN68 of Reference 7, but they have been adjusted slightly so that the effects of varying forward speed and rotor angular velocity can be seen independently. The adjusted flight conditions are denoted as DN66A, DN67A, and DN68A. Table I presents the shaft angles and the tip-path-plane positions required for trimmed flight at these conditions in addition to the advance ratios, forward velocities, and rotor angular velocities. The rotor planform used in the computations differs somewhat from the UH-1A configuration because of moving the blade root outboard, as discussed previously.

Figure 8 shows azimuthal variations in blade pitch angles (pitch control inputs plus torsional deflections) which are required to eliminate all nonsteady air loads (lift loading) through the twelfth harmonic. The plots which are shown for conditions DN66A and DN67A include only the variable part of the required pitch angles, and the mean angles required are given for each radial position. The forward velocity for condition DN66A is 17.3 percent less than the forward velocity for condition DN67A, but the rotor angular velocities for these conditions are the same.

Plots of the variable part of the required pitch angles are not presented for flight condition DN68A. The angular velocity for condition DN68A is 3.5 percent greater than the one for condition DN67A, while the forward velocities for the two cases are the same. The azimuthal plots for condition DN68A did not depart significantly from those shown on Figure 8 for condition DN67A and are not included to avoid confusing the curves. However, results for condition DN68A, which are included in the tabular data to be discussed, indicate differences in the harmonic content of the required pitch angles for conditions DN67A and DN68A.

Table I
PARAMETERS FOR ADJUSTED FLIGHT CONDITIONS

PARAMETERS	ADJUSTED FLIGHT CONDITION*		
	DN66A	DN67A	DN68A
V_f = FORWARD VELOCITY (ft/sec) (knots)	155.4 92.1	188.0 111.4	188.0 111.4
Ω = ROTOR ANGULAR VEL. (rad/sec) (rpm)	32.8 313	32.8 313	33.9 324
μ = ADVANCE RATIO	0.215	0.259	0.251
ρ = AIR DENSITY (slugs/ft ³)	0.002155	0.002155	0.002155
W_b = LOAD/BLADE (lb)	3200	3200	3200
α_s = SHAFT ANGLE (deg)	4.6	6.5	6.5
TIP-PATH-PLANE POSITION RELATIVE TO SHAFT:			
β_{1C} = FORWARD TILT (deg)	-0.74	-0.65	-0.65
β_{1S} = LEFT TILT (deg)	0.68	1.80	1.46

* THE ADJUSTED FLIGHT CONDITIONS DN66A, DN67A, AND DN68A ARE SLIGHTLY DIFFERENT FROM THE CORRESPONDING CONDITIONS OF REFERENCE 7.

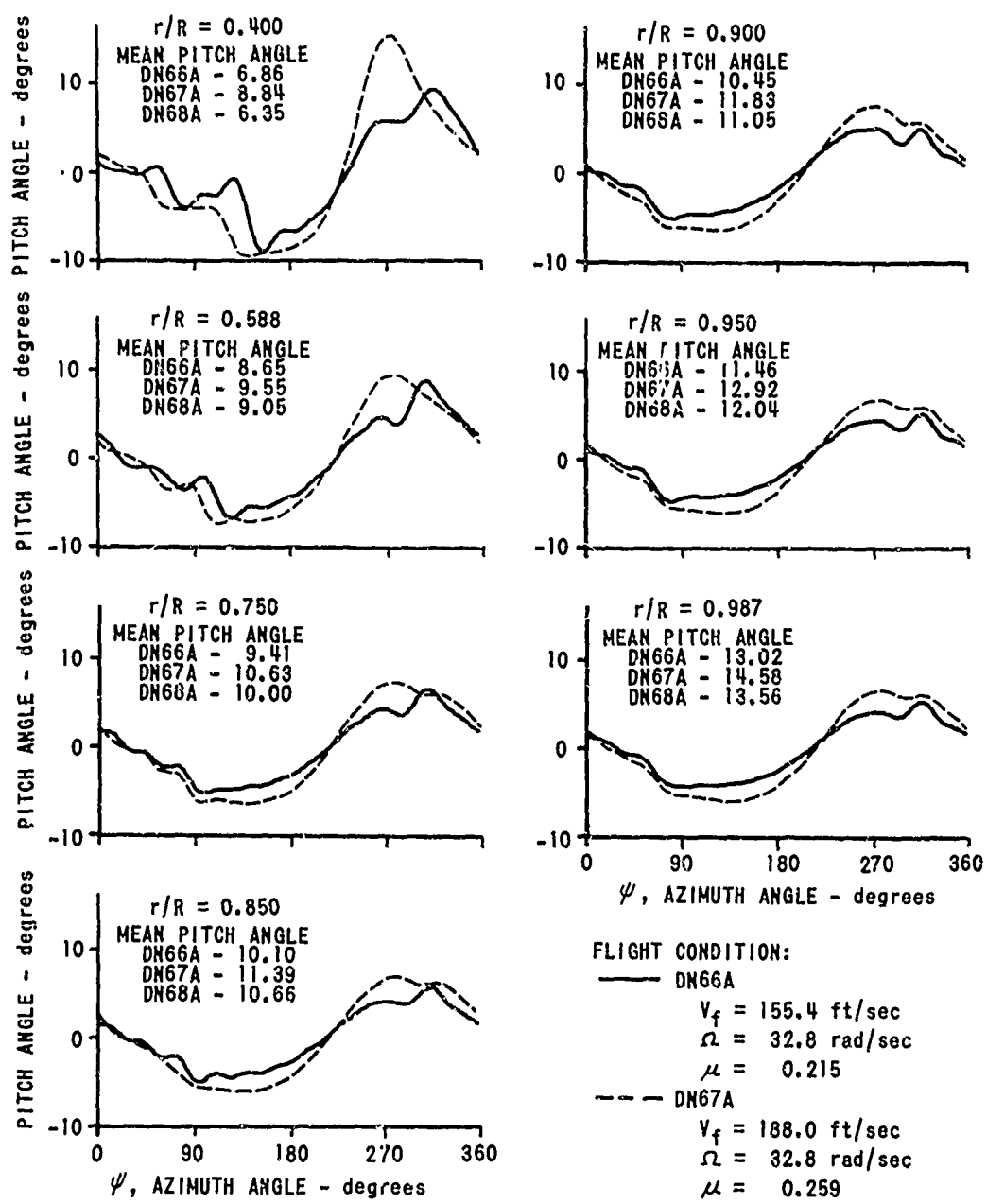


Figure 8 AZIMUTHAL VARIATIONS OF BLADE PITCH ANGLES REQUIRED TO ELIMINATE ALL HARMONIC AIR LOADS (MODIFIED UH-1A CONFIGURATION)

It can be seen from the plots on Figure 8 that ordinary first harmonic pitching motion is by far the largest harmonic component present. These first harmonic pitch changes are all of approximately the same magnitude with the exception of those at the most inboard station; they result primarily from the requirements on rotor tip-path-plane position. Second and higher harmonic components can be observed in the azimuthal variations of the required pitch angles but, in general, the curves appear fairly smooth except for irregularities found at the most inboard station.

In order that a more quantitative evaluation of the data can be made, the results of the harmonic analysis of the required blade pitch angles (i.e., the required geometric angles of attack) are presented in Table II. At the inboard station, $r/R = 0.400$, where large forward velocity variations occur, a second harmonic pitch angle change of 4.2 degrees is required for condition DN67A. The required second harmonic pitch variation is reduced to 2.1 degrees at the next outboard station ($r/R = 0.588$). For further outboard stations, the required second harmonic control inputs do not exceed 1.1 degrees.

The tables indicate that the required pitch control inputs at harmonics from the third to the fifth are of the order of 0.5 degree except for $r/R = 0.400$ where they reach 1.8 degrees. The required pitch angles for the sixth to the twelfth harmonics are considerably lower.

Although the plots for flight condition DN67A ($\Omega = 32.8 \text{ rad/sec}$) and flight condition DN68A ($\Omega = 33.9 \text{ rad/sec}$) were almost indistinguishable, it can be seen in Table II that small differences exist in both the amplitudes and phases of the pitch angles required to eliminate the various harmonic air loads. Much larger differences in the required amplitudes and phases of the pitch angles are found for the speed increment between flight condition DN66A ($V_f = 155.4 \text{ ft/sec}$) and flight condition DN67A ($V_f = 188.0 \text{ ft/sec}$).

In order to get a better idea of how the ideal control angles computed in this section might be approximated by an actual control mechanism, plots are presented on Figure 9 of required pitch angles versus radial position. The curves are presented for increments in azimuth angle of 30 degrees. Similar curves were also obtained for azimuth positions intermediate to the ones given but are not presented since they show the same trends as the other results. In Figure 9 as in Figure 8, results are given corresponding only to flight conditions DN66A and DN67A, since the results for DN68A were very close to those for DN67A.

Table II
HARMONIC ANALYSIS OF GEOMETRIC ANGLES OF ATTACK
REQUIRED TO ELIMINATE HARMONIC AIR LOADS

(a) $r/R = 0.400$

FLIGHT CONDITION	DN66A		DN67A		DN68A	
	HARMONIC	AMPLITUDE (degrees)	PHASE (degrees)	AMPLITUDE (degrees)	PHASE (degrees)	AMPLITUDE (degrees)
0	6.856	0.0	8.842	0.0	6.348	0.0
1	6.171	40.6	9.151	54.1	8.094	53.7
2	2.573	146.1	4.208	173.9	3.724	174.0
3	0.358	33.8	1.783	-84.0	1.484	-79.5
4	0.916	-178.1	1.254	-15.9	0.988	-24.0
5	1.192	138.3	0.648	152.6	0.702	151.9
6	0.543	-33.6	0.455	135.7	0.361	111.3
7	0.249	-103.9	0.172	-42.8	0.204	-62.6
8	0.359	32.6	0.034	138.1	0.136	125.0
9	0.341	-128.7	0.166	42.1	0.258	18.2
10	0.486	130.7	0.175	-60.8	0.274	-86.3
11	0.213	21.8	0.123	-147.7	0.178	165.8
12	0.102	-180.0	0.032	-180.0	0.086	0.0

(b) $r/R = 0.588$

0	8.652	0.0	9.548	0.0	9.045	0.0
1	5.856	51.5	7.419	58.0	6.731	57.4
2	1.056	149.0	2.095	-175.3	1.716	-178.0
3	0.664	114.1	0.610	-97.8	0.365	-99.3
4	0.243	135.7	0.367	37.2	0.367	55.8
5	0.579	-118.7	0.047	-114.0	0.088	-179.2
6	0.148	-28.6	0.346	-172.0	0.359	-178.7
7	0.662	10.8	0.271	123.3	0.246	119.4
8	0.226	-33.5	0.246	28.5	0.229	21.4
9	0.366	172.2	0.195	-56.6	0.193	-57.3
10	0.113	151.8	0.168	-143.4	0.155	-139.9
11	0.269	-67.2	0.104	115.8	0.082	122.2
12	0.013	0.0	0.080	0.0	0.052	0.0

AZIMUTHAL VARIATION OF REQUIRED n th HARMONIC ANGLE = (Ampl.) $\times \cos(n\psi + \text{Phase Angle})$

Table II
HARMONIC ANALYSIS OF GEOMETRIC ANGLES OF ATTACK
REQUIRED TO ELIMINATE HARMONIC AIR LOADS

(c) $r/R = 0.750$

FLIGHT CONDITION	DN66A		DN67A		DN68A	
	HARMONIC	AMPLITUDE (degrees)	PHASE (degrees)	AMPLITUDE (degrees)	PHASE (degrees)	AMPLITUDE (degrees)
0	9.411	0.0	10.630	0.0	9.995	0.0
1	4.994	58.4	6.788	59.0	6.108	58.6
2	0.366	161.0	1.130	-178.1	0.881	177.9
3	0.170	168.4	0.273	-74.6	0.149	-67.8
4	0.408	150.9	0.384	96.4	0.392	103.6
5	0.181	-108.6	0.259	104.7	0.223	113.0
6	0.404	-65.4	0.082	-151.8	0.110	-124.0
7	0.174	-40.1	0.153	-150.7	0.131	-126.2
8	0.198	72.8	0.083	121.6	0.061	64.1
9	0.114	83.5	0.167	30.4	0.205	26.4
10	0.154	-104.8	0.177	-21.8	0.160	-12.4
11	0.232	-112.7	0.132	-101.1	0.116	-118.5
12	0.098	-180.0	0.151	-180.0	0.172	-180.0

(d) $r/R = 0.850$

0	10.100	0.0	11.390	0.0	10.660	0.0
1	4.569	60.4	6.531	59.5	5.813	59.4
2	0.300	175.9	0.840	176.9	0.664	174.5
3	0.097	-158.6	0.226	-56.7	0.149	-53.9
4	0.351	153.5	0.283	108.8	0.288	118.5
5	0.132	-147.7	0.257	121.9	0.212	133.5
6	0.301	-71.6	0.052	159.1	0.062	-121.3
7	0.179	-67.4	0.095	-88.7	0.138	-75.8
8	0.116	74.6	0.074	-57.4	0.101	-36.1
9	0.175	63.8	0.075	11.0	0.115	17.7
10	0.079	-44.9	0.074	25.0	0.079	31.0
11	0.193	-120.6	0.009	41.9	0.045	171.4
12	0.198	-180.0	0.038	-180.0	0.113	-180.0

AZIMUTHAL VARIATION OF REQUIRED n th HARMONIC ANGLE = (Ampl.) $\times \cos(n\psi + \text{Phase Angle})$

Table 11
HARMONIC ANALYSIS OF GEOMETRIC ANGLES OF ATTACK
REQUIRED TO ELIMINATE HARMONIC AIR LOADS

(e) $r/R = 0.900$

FLIGHT CONDITION	DN66A		DN67A		DN68A		
	HARMONIC	AMPLITUDE (degrees)	PHASE (degrees)	AMPLITUDE (degrees)	PHASE (degrees)	AMPLITUDE (degrees)	PHASE (degrees)
0	10.450	0.0		11.830	0.0	11.050	0.0
1	4.446	63.5		6.396	61.1	5.671	61.2
2	0.156	-176.3		0.733	178.5	0.571	176.8
3	0.153	-63.0		0.252	-47.4	0.202	-46.0
4	0.347	170.2		0.231	121.9	0.232	133.1
5	0.293	177.1		0.277	135.1	0.251	144.7
6	0.104	-84.3		0.064	133.8	0.036	-166.5
7	0.240	-38.9		0.124	-54.3	0.165	-52.5
8	0.158	-28.4		0.149	-57.4	0.171	-48.0
9	0.044	69.4		0.050	-31.4	0.061	-17.2
10	0.110	124.3		0.076	81.8	0.081	91.6
11	0.094	138.6		0.081	86.8	0.091	117.7
12	0.066	-180.0		0.010	0.0	0.056	-180.0

(f) $r/R = 0.950$

0	11.460	0.0	12.920	0.0	12.040	0.0
1	4.496	67.9	6.484	64.9	5.734	65.1
2	0.189	-143.0	0.736	-173.1	0.577	-173.2
3	0.202	-53.0	0.268	-42.2	0.221	-41.3
4	0.331	170.1	0.204	120.1	0.207	137.3
5	0.345	168.2	0.260	140.0	0.246	149.0
6	0.052	-135.6	0.059	141.9	0.040	-178.8
7	0.249	-38.7	0.135	-52.0	0.170	-51.2
8	0.226	-38.8	0.167	-58.2	0.190	-52.1
9	0.021	32.1	0.051	-60.8	0.055	-38.4
10	0.183	115.4	0.076	98.6	0.091	104.4
11	0.175	113.4	0.092	93.0	0.108	112.8
12	0.047	-180.0	0.004	0.0	0.038	-180.0

AZIMUTHAL VARIATION OF REQUIRED n th HARMONIC ANGLE = (Ampl.) $\times \cos(n\psi + \text{Phase Angle})$

Table II
HARMONIC ANALYSIS OF GEOMETRIC ANGLES OF ATTACK
REQUIRED TO ELIMINATE HARMONIC AIR LOADS

(g) $r/R = 0.987$

FLIGHT CONDITION	DN66A		DN67A		DN68A	
	HARMONIC	AMPLITUDE (degrees)	PHASE (degrees)	AMPLITUDE (degrees)	PHASE (degrees)	AMPLITUDE (degrees)
0	13.020	0.0	14.580	0.0	13.560	0.0
1	4.833	75.7	6.905	72.3	6.106	72.7
2	0.379	-131.5	0.920	-159.5	0.743	-158.6
3	0.232	-45.2	0.337	-36.3	0.279	-36.0
4	0.303	166.0	0.181	122.1	0.184	125.6
5	0.341	166.6	0.243	145.0	0.236	153.2
6	0.071	-156.7	0.068	158.6	0.058	-170.0
7	0.222	-41.3	0.120	-55.9	0.152	-54.2
8	0.226	-37.0	0.157	-55.1	0.178	-49.8
9	0.053	19.8	0.059	-51.2	0.061	-39.0
10	0.177	109.1	0.062	97.6	0.078	104.4
11	0.183	116.3	0.082	102.5	0.101	118.5
12	0.074	-180.0	0.018	-180.0	0.057	-180.0

AZIMUTHAL VARIATION OF REQUIRED n th HARMONIC ANGLE = (Ampl.) $\times \cos(n\psi + \text{Phase Angle})$

It is seen from the curves on Figure 9 that the radial variation of required pitch angles at each azimuth position can be fitted quite well with one or two straight-line segments in the case of the higher speed flight condition DN67A. However, such a representation of the curves for condition DN66A is less satisfactory because some of them exhibit a pronounced "S" shape.

Figure 10 is presented in order to show the mean pitch angle versus radius distributions found in the computations for the required pitch angles to eliminate all harmonic air loads. It can be seen that the appropriate mean twist distribution varies with the flight regime. Consequently, designing for the entire flight spectrum would necessitate selecting a built-in blade twist distribution which would be a compromise between the distributions required for low- and high-speed flight. The increments in mean twist from the built-in twist as required for different flight conditions would place additional demands on the blade pitch angle control system.

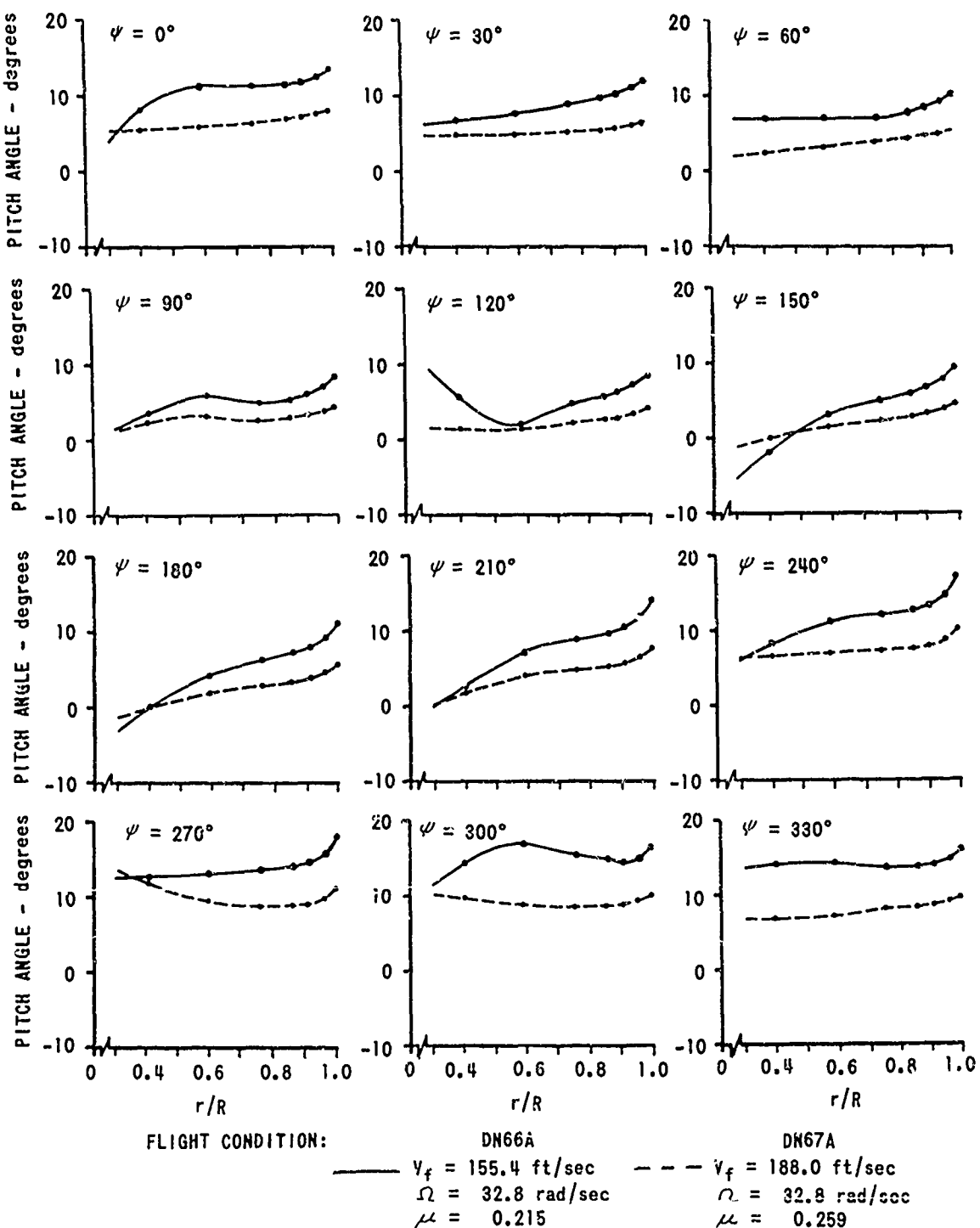


Figure 9 RADIAL VARIATION OF BLADE PITCH ANGLES REQUIRED TO ELIMINATE ALL HARMONIC AIR LOADS (MODIFIED UH-1A CONFIGURATION)

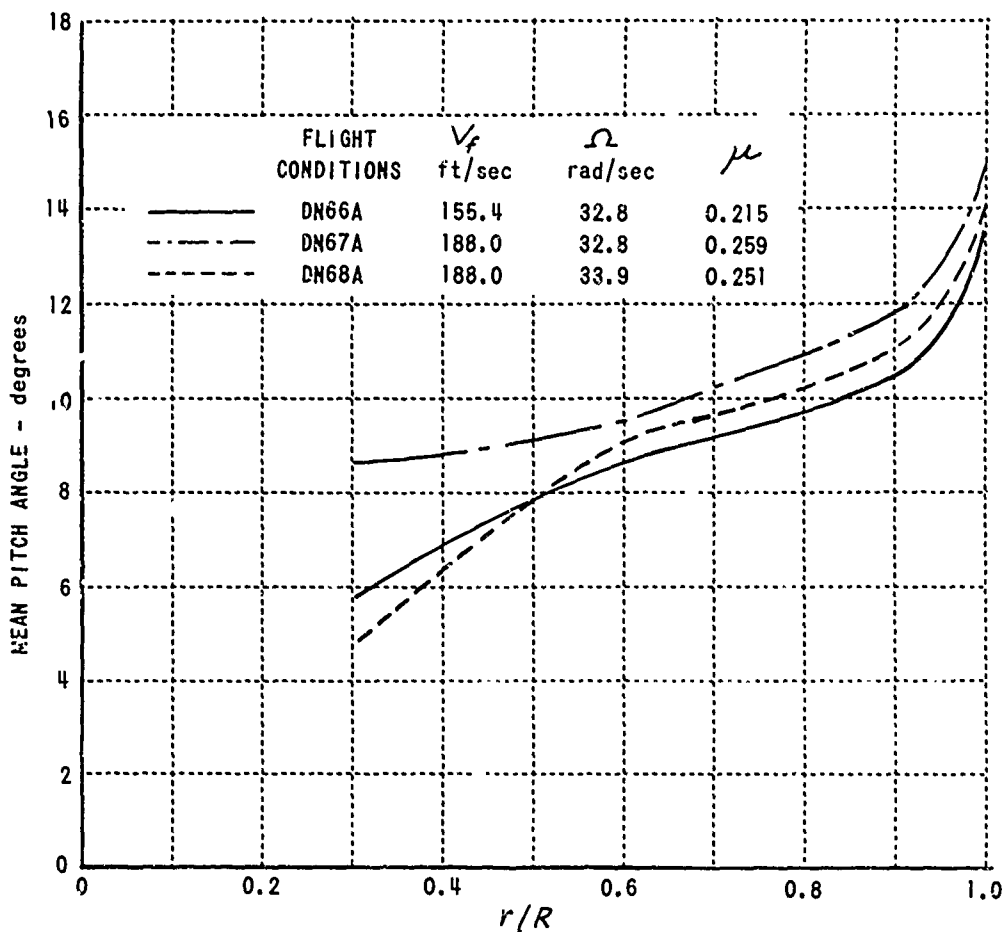


Figure 10 REQUIRED MEAN PITCH ANGLE VERSUS RADIUS DISTRIBUTION TO ELIMINATE ALL HARMONIC AIR LOADS

The large positive twist distribution indicated on Figure 10 is in marked contrast with present design practice in which a negative twist distribution is used. It should be emphasized that the required positive twist distributions which were computed are a direct consequence of the specified lift distribution shown on Figure 7. This lift distribution had an unusually high tip loading. A positive mean twist distribution is not a general characteristic of the pitch angle inputs required to obtain an azimuthally independent lift distribution.

3. METHOD FOR FINDING PITCH ANGLE INPUTS TO ELIMINATE OSCILLATORY ROOT SHEARS

In the preceding section, the blade pitch angle variations were found which are necessary to eliminate all harmonic lift loads on a rotor and, consequently, all harmonic shears at the blade root. A method is considered in this section for finding the pitch angle inputs to satisfy the less severe requirements for eliminating only oscillatory vertical root shears. The continuous radial variation of pitch angle control which was used in Section 2 is no longer assumed, and the root shears must be made zero without making all harmonic air loads zero. The blade dynamic motions excited by these residual harmonic air loads affect the root shears and are included in the analysis.

In particular, a computational procedure is developed for finding required harmonic control inputs in the case of the two-blade teetering rotor assuming:

1. The flight condition is steady so that blade dynamic motions can be assumed periodic.
2. The blade root shears due to combined lift and inertia force loadings are to be zero at prescribed harmonics.
3. The tip-path plane is in a prescribed position.
4. The blade dynamic motions can be described by:
 - a. Three symmetrical bending modes.
 - b. Teetering motion, and two antisymmetrical bending modes.
 - c. Two symmetrical torsional modes.
 - d. Two antisymmetrical torsion modes (with the same frequencies as the symmetric modes).
5. Control is applied by:
 - a. One symmetric mode and one antisymmetric control mode, each giving uniform feathering along the blade span.

- b. One symmetric mode and one antisymmetric control mode, each giving differential feathering of the inboard and outboard sections of the blade.

When the second and all higher even harmonic root shears are prescribed to be zero, the vertical root shear transmitted to the fuselage is a constant, not depending on azimuth position. The computational procedure can, in principle, be used for finding the pitch inputs required to eliminate canceling root shears which occur at odd harmonics for the teetering rotor, but numerical results for this case are not presented.

The aerodynamic forces to be used in the computational procedure of this section are those discussed in Section 1 without the simplifying assumptions made in Section 2. Thus, reversed flow and stall effects are to be taken into account by the methods described in Reference 6.

DESCRIPTION OF ROTOR DYNAMIC MOTIONS

The dynamic motion of the rotor is described by the modes indicated schematically in Figure 11 which are applicable for the case of a two-bladed teetering configuration. All of these modes can be handled simultaneously in the computer program which has been developed; however, in general, solutions were obtained by setting some of the generalized coordinates for these modes equal to zero. The computational procedure which was developed is also capable of treating the case of the three-bladed articulated rotor. The same basic procedure could be used for rotors having a larger number of blades but would require some modification of the computer program.

It can be seen that even and odd subscripts are used to designate symmetric and antisymmetric modes respectively. The vertical tip deflections due to bending in the first, second, and third symmetric bending modes are denoted by h_2 , h_4 , and h_6 and are used as generalized coordinates. Similarly, the tip deflections h_1 , h_3 , and h_5 are used as generalized coordinates for the teetering, first antisymmetric bending, and second antisymmetric bending modes.

It will be noted that a vertical rotor displacement mode is included corresponding to vertical motion of the flapping hinge produced by fuselage and hub motion. The h_{05} mode is introduced because the sum of the generalized aerodynamic and inertia forces acting in this degree of freedom is equal in magnitude to the transmitted shear. However, the amplitude of the h_{05} motion is assumed to be zero throughout the analysis.

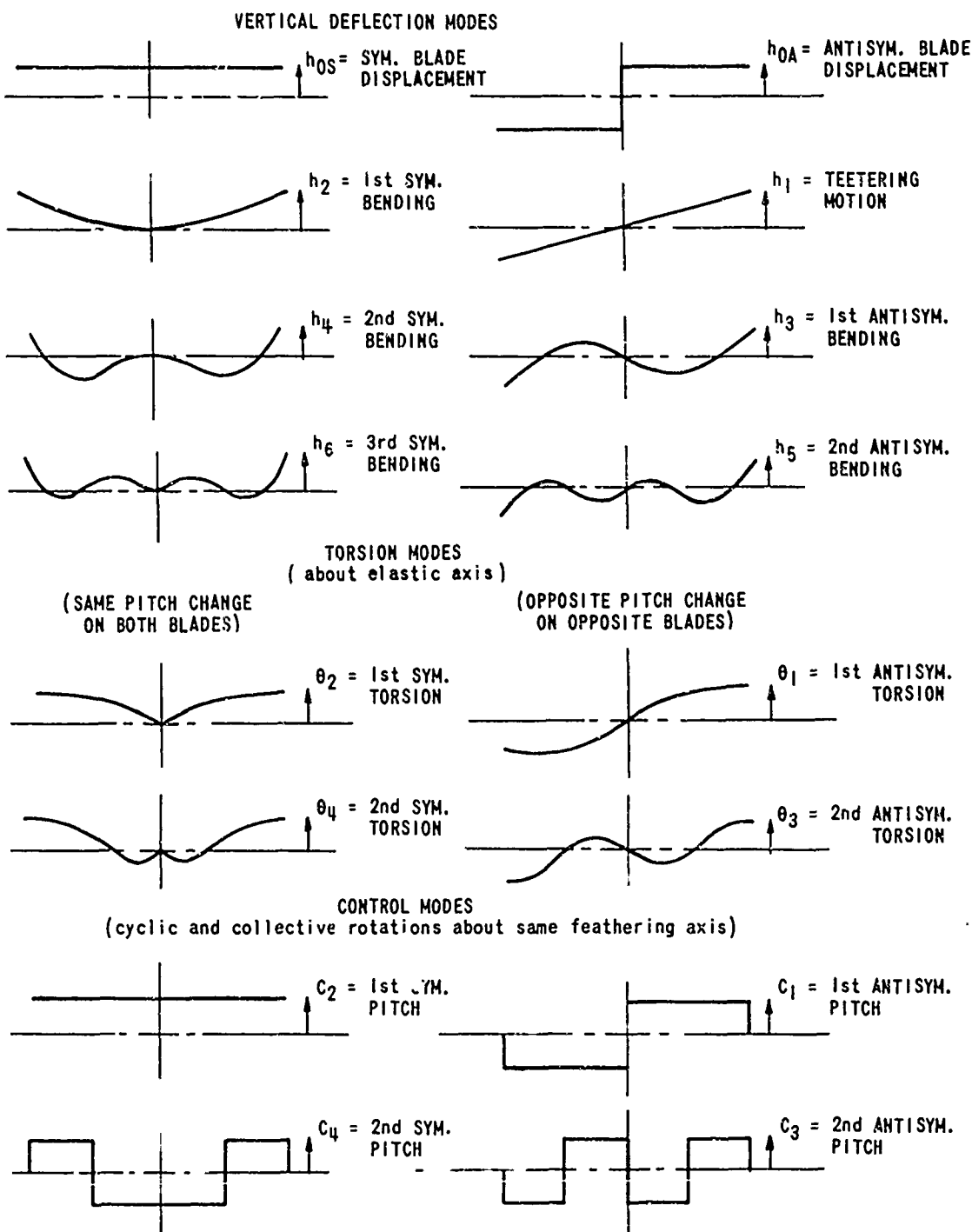


Figure 11 SCHEMATIC DIAGRAM OF MODES USED TO DESCRIBE MOTIONS OF A TWO-BLADED TEEETERING ROTOR

An antisymmetric blade displacement mode (h_{04}) is also shown in the figure. This mode has no physical significance in the case of a teetering rotor, and motions in this mode are assumed to be zero. In the case of an articulated rotor blade with an offset flapping hinge, this mode corresponds to a tilting of the shaft. The generalized forces acting in the antisymmetric h_{04} mode produce canceling root shears, but such shears can transmit moments to the shaft when offset hinges are used.

The generalized coordinates θ_1 , θ_2 , θ_3 , and θ_4 used for the blade torsion modes are the angular deflections about the elastic axis at the blade tip. Since the pitching of the blade root is described by the control modes, the angular deflections in the blade torsion modes are assumed to be zero at the blade root. As a result, the deflection shapes for each blade are the same for the symmetric and antisymmetric torsional modes. The natural frequencies of the bending and torsional modes indicated on Figure 11 are presented in Appendix I for the configuration studied.

The computational model permits the use of two symmetric and two antisymmetric control modes. Ordinary collective pitch is the steady component of the motion in the first symmetric control mode, c_1 , while ordinary cyclic pitch is the first harmonic motion in the first antisymmetric control mode, c_2 . Higher harmonic motions can be introduced in both the c_1 and c_2 modes in order to modify the root shears. The second symmetric and antisymmetric control modes, c_3 and c_4 , which are shown schematically, are possible differential control motions in which the inner and outer sections of the blade pitch in opposite directions. The mode shapes shown for c_3 and c_4 could be replaced by other radial variations within the framework of the analysis. For example, a linear variation in pitch might be used which could be produced by a device introducing a moment at the blade tip.

The spanwise variations of the amplitudes in each mode are represented by dimensionless f functions. Thus,

$$f_{g_i}(r)g_i(t) = \text{amplitude of motion in } g_i^{\text{th}} \text{ mode at radial station, } r, \text{ and time, } t.$$

HARMONIC AND DISCRETE TIME TREATMENT OF VARIABLES

The investigation has been limited to considering steady flight conditions for which the rotor loads, rotor motions and transmitted shears are assumed to be periodic. However, in carrying out the aerodynamic computations, including the effects of the wake vorticity distribution, it is convenient to utilize the values of the variables at discrete time increments similar to the treatment used in Reference 6. As discussed in Section 1, the positions of the shed and trailing vortices

in the wake are determined from uniform inflow theory for the given flight condition. Then, when the values of V_r , α , $\dot{\alpha}$ and h in Equation (12) are given at the NRA blade segment positions in the rotor disk, the aerodynamic problem is completely defined. The solution to this aerodynamic problem gives the blade circulation, lift, and pitching moment at each of the blade segment positions which is equivalent to giving the variations in the aerodynamic loadings at discrete azimuth or time increments. The transmitted shears and generalized forces acting in each of the bending and torsional modes at the discrete azimuth positions can be computed from the lift and moment distributions. In computing the dynamic responses to periodic forces, however, it is desirable to use a harmonic description of the variables. The time variation of the q_i^{th} generalized coordinate can be approximated by a finite Fourier series as follows:

$$q_i(t) = \sum_{n=0}^{\frac{1}{2}(NA)} \left\{ (A_n q_i) \cos n\psi + (B_n q_i) \sin n\psi \right\} \quad (30)$$

where
$$\begin{aligned} (A_0 q_i) &= \frac{1}{(NA)} \sum_{k=1}^{(NA)} (q_i)_k, \\ (A_n q_i) &= \frac{2}{(NA)} \sum_{k=1}^{(NA)} (q_i)_k \cos n\psi_k \\ (B_n q_i) &= \frac{2}{(NA)} \sum_{k=1}^{(NA)} (q_i)_k \sin n\psi_k \end{aligned} \quad \left. \begin{aligned} n &= 1 \text{ to } \left(\frac{NA}{2} - 1\right), \\ (A_{\frac{1}{2}(NA)} q_i) &= \frac{1}{(NA)} \sum_{k=1}^{(NA)} (q_i)_k \cos(k-1)\pi. \end{aligned} \right\} \quad (31)$$

The symbol $(A_n q_i)$ indicates the operation of multiplying $(q_i)_k$, the value of the generalized coordinate at azimuth position, $\psi_k = 2\pi(k-1)/(NA)$, by $(2/(NA))\cos n\psi_k$ and summing for (NA) equally spaced azimuth positions. This is simply the coefficient of the n^{th} harmonic cosine term. Similarly, $(B_n q_i)$ is the coefficient of the n^{th} harmonic sine term.

DISCUSSION OF EQUATIONS OF MOTION AND ANALYTICAL PROBLEM

The equation of motion for each of the linear deflection and torsional modes can be written in the general form,

$$\begin{aligned} \sum_j \left\{ M_{q_i q_j} \ddot{q}_j - 2\Omega G_{q_i q_j} \dot{\bar{q}}_j + (K_{q_i q_j} - \Omega^2 T_{q_i q_j}) \bar{q}_j + i(gK)_{q_i q_j} (\bar{q}_j \cdot \bar{q}_{j, AVG}) \right\} \\ = \bar{G}_{q_i} + \bar{Z}_{q_i} + \delta_{q_i, h_{os}} \bar{S}_N + \delta_{q_i, h_{oA}} \bar{S}_C, \end{aligned} \quad (32)$$

for assumed complex periodic variations in the generalized coordinates and in all the generalized forces acting on the blade. In this expression, the $M_{q_i q_j}$'s are generalized mass coefficients, the $G_{q_i q_j}$'s are gyroscopic coupling coefficients, the $K_{q_i q_j}$'s are generalized stiffness coefficients, the $T_{q_i q_j}$'s are centrifugal force coefficients, and the $\delta_{q_i q_j}$'s are structural damping coefficients. Definitions of these coefficients are given in Appendix I. The quantities on the right-hand side are the complex generalized aerodynamic force acting in the q_i th mode, \bar{G}_{q_i} ; the generalized centrifugal force arising from built-in twist and preconing, \bar{Z}_{q_i} ; the complex noncanceling root shear, \bar{S}_N ; and the complex canceling root shear, \bar{S}_C . The shears, S_N and S_C , act only in the h_{os} and h_{OA} modes, respectively, as indicated by the δ functions. All coefficients and generalized forces are the values per blade.

Complex vectors (indicated by bars) have been used in Equation (32), since they are convenient in writing the conventional expression for structural damping. The complex periodic variations of each generalized coordinate (q_i) is expressed in the form,

$$\begin{aligned}\bar{q}_i &= \sum_{n=0}^{\frac{1}{2}(NA)} \left\{ (A_n q_i) - i(B_n q_i) \right\} e^{i\omega t} \\ &= \sum_{n=0}^{\frac{1}{2}(NA)} \left\{ (A_n q_i) \cos n\psi + (B_n q_i) \sin n\psi \right\} + i \sum_{n=0}^{\frac{1}{2}(NA)} \left\{ -(B_n q_i) \cos n\psi + (A_n q_i) \sin n\psi \right\},\end{aligned}\quad (33)$$

where the complex coefficients have been defined in such a manner that the real part of Equation (33) is identical to Equation (30). Similar expressions hold for the other complex periodic quantities (\bar{G}_{q_i} , \bar{Z}_{q_i} , \bar{S}_N , and \bar{S}_C).

Only the real part of Equation (32) is considered in the subsequent discussion because it suffices to describe the real physical motion. After substituting expressions of the type shown in Equation (33), the real part of Equation (32) can be arranged in the form of a sum of harmonic terms, and the coefficient of each cosine and sine harmonic must vanish for the complete equation to be satisfied. The requirements on the coefficients of $\cos n\psi$ and $\sin n\psi$ in the equation for the q_i th mode are

$$\begin{aligned}\sum_j \left\{ K_{q_i q_j} - \Omega^2 T_{q_i q_j} - n^2 \Omega^2 M_{q_i q_j} \right\} (A_n q_j) + \sum_j \left\{ (Kg)_{q_i q_j} - n \Omega^2 G_{q_i q_j} \right\} (B_n q_j) \\ + \delta_{q_i, h_{os}} (A_n S_N) + \delta_{q_i, h_{OA}} (A_n S_C) = (A_n G_{q_i}) + (A_n Z_{q_i}),\end{aligned}\quad (34)$$

$$\begin{aligned}- \sum_j \left\{ (Kg)_{q_i q_j} - n \Omega^2 G_{q_i q_j} \right\} (A_n q_j) + \sum_j \left\{ K_{q_i q_j} - \Omega^2 T_{q_i q_j} - n^2 \Omega^2 M_{q_i q_j} \right\} (B_n q_j) \\ + \delta_{q_i, h_{os}} (B_n S_N) + \delta_{q_i, h_{OA}} (B_n S_C) = (B_n G_{q_i}).\end{aligned}\quad (35)$$

In order to clarify the problem, these equations and certain auxiliary constraint equations are displayed in matrix form below.

Form of equations for even harmonics, $n = 2, 4, \dots, 12$ (also applicable for $n = 0$ as discussed below):

Form of equations for odd harmonics, $n = 1, 3, \dots, 11$:

$D(I, J, n) =$	$D(I, J, n)$	$(A_n S_C)$	$(A_n G_{h_{nA}})$	0
$0 \left[\frac{K q_i q_j}{n^2} - n^2 M_{q_i q_j} - T_{q_i q_j} \right] 0$	$\left[\frac{(Kg) q_i q_j}{n^2} - 2nG_{q_i q_j} \right]$	(h_1)	(G_{h_1})	\cdot
$D(I, J, n) = 1/n^2 \text{ (if } J = JP(n, I))$	$= 0 \text{ (otherwise)}$	(h_3)	(G_{h_3})	0
$D(I, J, n) = -D(I-2, J+2, n)$	$D(I, J, n)$	(h_s)	(G_{h_s})	0
$D(I, J, n) = 1/n^2 \text{ (if } J = JP(n, I))$	$= 0 \text{ (otherwise)}$	(θ_1)	(G_{θ_1})	0
		(θ_3)	(G_{θ_3})	0
		(c_1)	(G_{c_1})	0
		(c_3)	(G_{c_3})	$\frac{1}{n^2} YP(n, 7)$
		$= \frac{1}{n^2} (0)$	(0)	$\frac{1}{n^2} YP(n, 8)$
$B_n S_C$	$(B_n G_{h_{nA}})$	$(B_n h_{nA})$	$(B_n G_{h_{nA}})$	0
(h_1)	(G_{h_1})	(G_{h_1})	(G_{h_1})	0
(h_3)	(G_{h_3})	(G_{h_3})	(G_{h_3})	0
(h_s)	(G_{h_s})	(G_{h_s})	(G_{h_s})	0
(θ_1)	(G_{θ_1})	(G_{θ_1})	(G_{θ_1})	\cdot
(θ_3)	(G_{θ_3})	(G_{θ_3})	(G_{θ_3})	0
(c_1)	(G_{c_1})	(0)	(0)	$YP(n, 13)$
(c_3)	(G_{c_3})	(0)	(0)	$YP(n, 14)$

It follows from the symmetry of the two-bladed teetering rotor that the generalized forces acting in the symmetric modes can only be of even or zero harmonic order while those acting in the antisymmetric modes can only be of odd harmonic order. As a result, the response in the symmetric modes must be at zero or even harmonic orders, and the response in the antisymmetric modes must be at odd harmonics as indicated by the variables appearing on the left-hand sides of Equations (36) and (37). However, this does not mean that the two sets of equations are decoupled, because coupling can take place between harmonic coefficients of all orders through the generalized aerodynamic forces. For example, the combination of even harmonic blade motion and the flow dissymmetry due to forward flight can produce odd harmonic generalized aerodynamic forces.

The first four rows in Equation (36) represent the equilibrium of the n^{th} harmonic cosine components of the generalized forces in the symmetric vertical deflection modes (h_{0S}, h_2, h_4, h_6). The fifth and sixth rows represent the equilibrium of the cosine components of the generalized forces in the symmetric torsion modes (θ_2, θ_4). Similarly, the ninth to the fourteenth rows represent the equilibrium of the sine components of the generalized forces in the symmetric vertical deflection and torsional modes.

Sixteen variables are listed in the column matrix on the left-hand side of Equation (36). The deflections in the h_{0S} mode are assumed to be zero, but the noncanceling harmonic shear coefficients, ($A_n S_N$) and ($B_n S_N$), which are associated with this mode are treated as variables in the problem. The remaining variables are the sine and cosine components of the deflections in the symmetric bending modes, symmetric torsion modes, and symmetric control modes. There are no equations of motion included for the equilibrium of the control modes, since the characteristics of the control system have not been included in the study. The seventh, eighth, fifteenth, and sixteenth rows of Equation (36) are four constraint equations which are added to the dynamic equations to make the number of equations equal to the number of unknowns in the column matrix on the left-hand side. Since constraint equations are included in the equation set for each harmonic, a well-defined problem results for the complete system of equations having the same number of equations as unknowns.

The implementation of a pitch control system for the elimination of root shears might be based on several different concepts. One such system might apply a higher harmonic pitch control schedule which would be selected in accordance with the flight condition (i. e., flight velocity, rotor rpm, etc.). Solutions based on the method given in this section indicate the pitch control schedules which should be used. In another possible system, the output of a sensor measuring the blade root shears might be used as a feedback in a pitch control servo. The application of such a servo system would be dependent upon obtaining a design in

which the dynamic motions of the coupled rotor-servo system would be stable. A more extensive computer program would be required to study this problem, including the dynamics of both the rotor and servo systems.

A general element of the 16×16 dynamic response matrix on the left-hand side of Equation (36) is denoted by $D(I, J, n)$, where I and J indicate the row and column, respectively, and n the applicable harmonic order. The $[D]$ matrix has been partitioned, and the forms of typical elements in the submatrices are shown.

The n^{th} harmonic generalized aerodynamic forces acting in the symmetric modes are listed in the first column matrix on the right-hand side of Equation (36). In the next column matrix, a list is given of the generalized centrifugal forces ($Z_{q_i}(n)$) associated with preconing and built-in twist. These are steady forces and $Z_{q_i}(n)$ is zero unless $n = 0$. The last column on the right-hand side of Equation (36) is used in the computer program to prescribe the values of four variables (for $n = 0$, only two of the cosine coefficients need be prescribed, since all the sine coefficients are zero).

An example will be considered in order to clarify the meaning of the notation used in the constraint equations. If it were desired to use the seventh equation to put a constraint on $(A_n S_N)$ (i. e., the n^{th} harmonic cosine coefficient of noncanceling root shear), a setting,

$$YP(n, I = 7) = 1, \quad (38)$$

would be used in the inputs to the computer program. This means the only element of the $[D]$ matrix in the seventh row ($I = 7$) would be in the first column ($J = 1$) resulting in the equation

$$\frac{1}{\Omega^2} (A_n S_N) = \frac{1}{\Omega^2} YP(n, 7). \quad (39)$$

The input $YP(n, 7)$ would be set equal to zero if a solution were desired with the n^{th} harmonic noncanceling root shear equal to zero.

The preceding discussion has been given relative to the even harmonic equations, but analogous considerations hold for the odd harmonic equations. Although the expressions for the matrix elements appear to be the same in Equations (36) and (37), different $K_{q_i q_j}$, $M_{q_i q_j}$, $T_{q_i q_j}$, $(K_g)_{q_i q_j}$ and $G_{q_i q_j}$ coefficients are involved, because symmetric and antisymmetric modes occur in the two cases, respectively. For $n=0$, there are no sine component generalized forces or generalized coordinates and somewhat different treatment is required. It was desired to use matrices of the same order for all harmonics for convenience in the computer program. The $n=0$ case was brought into this framework by retaining only diagonal terms in the ninth to sixteenth rows of the matrix and setting the

right-hand side of the ninth to the sixteenth equations equal to zero. Thus, the same matrix inversion program could be used for $n=0$ as for the other harmonics.

The set of equations of motion and constraint equations for even or odd harmonics can be written symbolically in the form

$$[D(I, J, n)][X(n, J)] = \frac{1}{\Omega^2} [G(n, I)] + \frac{1}{\Omega^2} [Z(n, I)] + \frac{1}{\Omega^2} [YF(n, I)], \quad (40)$$

where appropriate symbols have been introduced for the column matrices in Equations (36) and (37). The $[X(n, J)]$ matrix is composed of variables corresponding to symmetric modes for zero and even harmonics and is composed of variables corresponding to antisymmetric modes for odd harmonics. The n^{th} harmonic generalized aerodynamic forces are functions of the lift and moments on the blade, which depend on all the harmonics of the motion as mentioned previously. That is,

$$[G(n, I)] = [f\{(A_0 h_2), \dots (A_0 c_4); (A_1 h_1), \dots (A_1 c_3); (B_1 h_1), \dots (B_1 c_3); \dots; (A_{12} h_2), \dots (A_{12} c_4)\}]. \quad (41)$$

An explicit expression for the generalized forces in the form of Equation (41) is not available, but such a relationship can be obtained from the solution of the aerodynamic problem as discussed in Section 1. For given harmonic coefficients, the azimuthal variations of the generalized coordinates can be computed using Equation (30). The input variables α , $\dot{\alpha}$, and h in Equation (12) can then be expressed in terms of the generalized coordinates for blade motion by referring to Figure 4 and again making small angle approximations. The geometric angle of attack at each blade segment position k relative to the local velocity v_{f_k} is

$$\alpha_k = \left\{ \theta_B + \sum_{\tau} f_{c_{\tau}} c_{\tau} \right\}_k \quad (42)$$

where θ_B is the built-in twist and the control modes are as shown on Figure 11. The relative angular velocity due to the motion of the blade is

$$\dot{\alpha}_k = \left\{ \sum_{\tau} f_{c_{\tau}} \dot{c}_{\tau} + \sum_{\gamma} f_{\theta_{\gamma}} \dot{\theta}_{\gamma} + \Omega \left(\beta_c + \sum_s h_s \frac{df_{h_s}}{dr} \right) \right\}_k. \quad (43)$$

The last term is due to the small component of the shaft angular velocity along the blade axis and was neglected in most of the computations. The vertical velocity of the airfoil relative to the air is

$$\begin{aligned}\dot{h}_k = & \left\{ V_f \sin \alpha_s + (V_f \cos \alpha_s) (\cos \psi) \left(\beta_c + \sum_s \dot{h}_s \frac{df_{h_s}}{dr} \right) \right. \\ & \left. + \sum_s \dot{h}_s f_{h_s} - e \sum_\tau \dot{\theta}_\tau f_{\theta_\tau} - e_o \sum_\tau \dot{c}_\tau f_{c_\tau} \right\}_k, \quad (44)\end{aligned}$$

where e is the distance between the midchord and elastic axis and e_o is the distance between the midchord and the pitch axis. The summations in Equations (42), (43), and (44) are over all the symmetric and antisymmetric modes of bending, torsion, or control motion.

Having determined the α_k 's, $\dot{\alpha}_k$'s and \dot{h}_k 's, Equation (11) can be solved for the bound vortices at all blade segment positions in the rotor disk, the corresponding Glauert coefficients can be evaluated, and the lift and pitching moment loadings (ℓ and η) can be computed by Equations (15) and (16). It is then a simple computation to determine the generalized forces in each of the vertical displacement and torsional modes from the relations

$$(G_{h_i})_k = \int \ell_k(r) f_{h_i}(r) dr \quad (45)$$

and

$$(G_{\theta_i})_k = \int (\eta - e\ell)_k f_{\theta_i}(r) dr, \quad (46)$$

where the subscript k indicates the generalized forces at azimuth angle ψ_k . The harmonic analysis of the results obtained from Equations (45) and (46) is the final step in relating the harmonic coefficients of the generalized aerodynamic forces and the harmonic coefficients of the generalized coordinates of the blade motions as indicated in Equation (41).

Figure 12 is a schematic diagram of the analytical problem which must be solved to find the pitch angle inputs necessary to eliminate oscillatory root shears. The purpose of this diagram is to show how the various parts of the problem are related in the approach which has been discussed. The overall diagram is divided into two boxes, one showing the solution for the aerodynamics of the rotor-wake system and the other, the solution for the dynamic blade response, required pitch

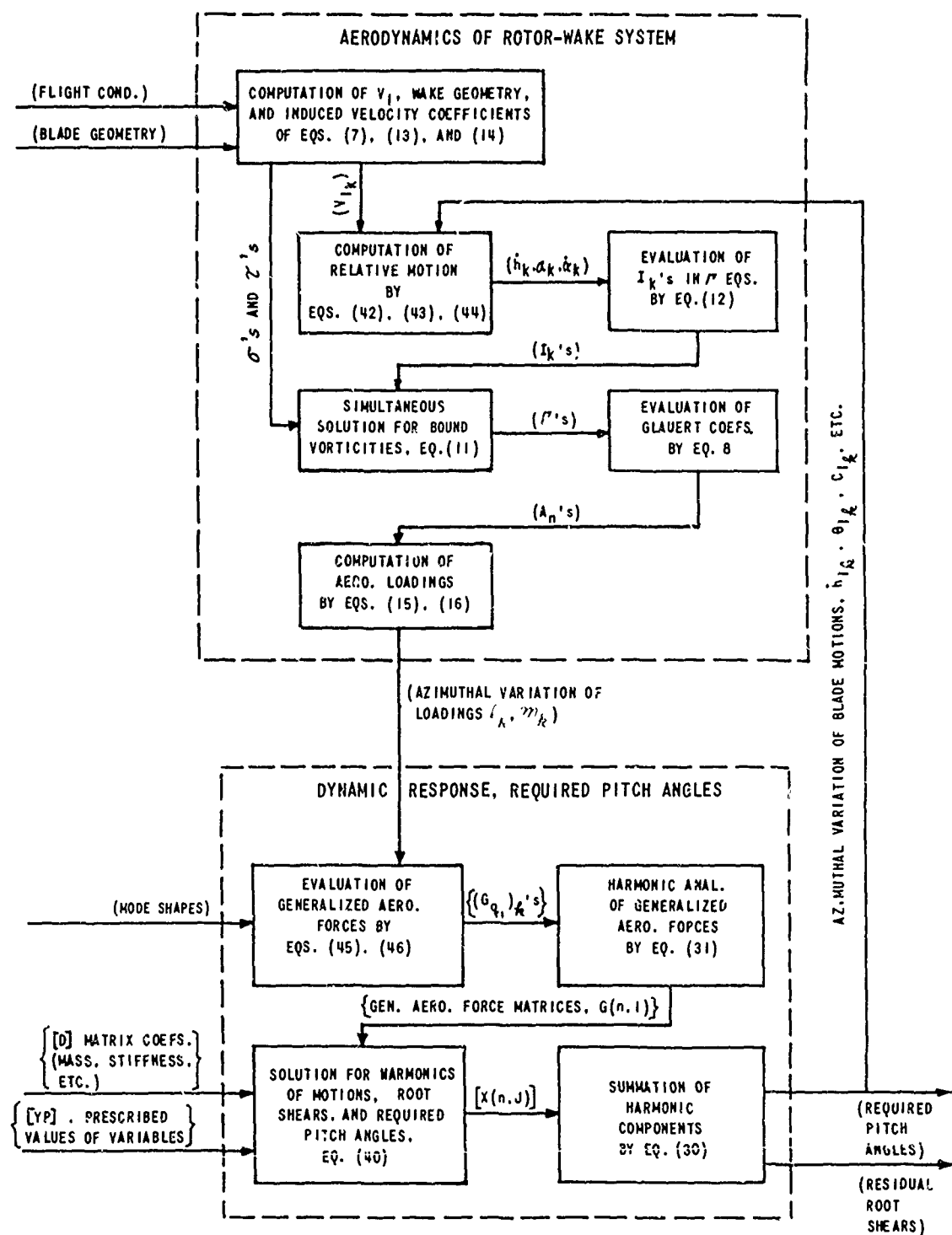


Figure 12 SCHEMATIC DIAGRAM OF THE ANALYTICAL PROBLEM OF FINDING PITCH ANGLE INPUTS TO ELIMINATE OSCILLATORY ROOT SHEARS

angles, and residual root shears. It is again pointed out that the aerodynamic part of the problem is treated by using the values of the variables at discrete time or azimuth angle increments, while the solutions for the dynamics motion and shears are treated in terms of their harmonic coefficients.

ITERATIVE SCHEME OF SOLUTION FOR HARMONIC MOTIONS AND ROOT SHEARS

It is evident from the schematic diagram shown on Figure 12 that the dependencies of the aerodynamic loadings on the dynamic blade motions are very involved. The loads for specified input motions are obtained only after an iterative solution for the bound vortices as discussed in Section 1. Consequently, a direct solution for the harmonic blade motions and root shears due to the aerodynamic loadings cannot be carried out, and an iterative scheme of solution must also be adopted for their determination.

In discussing this iterative scheme of solution, superscripts are used to denote the values of the variables in a particular iteration. Equation (40) can then be written as

$$[D(I, J, n)] [X^{(t)}(n, J)] = \frac{1}{\Omega^2} [G^{(t-1)}(n, I)] + \frac{1}{\Omega^2} \Delta^{(t)} [G(n, I)] + \frac{1}{\Omega^2} [Z(n, I)] + \frac{1}{\Omega^2} [Y_P(n, I)], \quad (47)$$

where $[X^{(t)}(n, J)]$ is the t^{th} approximation for the column matrix of variables; $[G^{(t-1)}(n, I)]$ is the column matrix of generalized aerodynamic forces based on the preceding approximation for the column matrix of variables; and $\Delta^{(t)}[G(n, I)]$ is the increment in the column matrix of generalized forces from the $(t-1)^{th}$ to the t^{th} approximation. That is,

$$\Delta^{(t)} [G(n, I)] = [G^{(t)}(n, I)] - [G^{(t-1)}(n, I)]. \quad (48)$$

No superscripts are shown for the $[D]$, $[Z]$, and $[Y_P]$ matrices because they remain constant in the iterative solution.

A possible iterative procedure would be to assume $\Delta^{(t)}[G]$ zero in computing the t^{th} approximation for the column matrix of variables, $[X^{(t)}]$, and to use these variables to compute the t^{th} approximation for the generalized aerodynamic forces, $[G^{(t)}]$; these, in turn, are used to compute $[X^{(t+1)}]$ neglecting $\Delta^{(t+1)}[G]$, etc. However, better convergence of the solution would be expected if a reasonable estimate could be made of the increments in the generalized aerodynamic forces from iteration to iteration. A relatively simple estimate of $\Delta^{(t)}[G]$ can be based on the assumption that the changes in the aerodynamic lifts and pitching moments from one iteration to the next are a linear function

of the corresponding changes in the harmonic coefficients of the blade motions. Accordingly, $\Delta^{(t)}[G]$ is approximated by an expression of the following form:

$$\begin{aligned} \frac{I}{\Omega^2} \Delta^{(t)}[G(n, I)] &= -[E(I, J, n)] \{ [X^{(t)}(n, J)] - [X^{(t-1)}(n, J)] \} \\ &\quad + \frac{\mu}{2} [L(I, J, n)] \{ [X^{(t)}(n-1, J)] - [X^{(t-1)}(n-1, J)] \} \\ &\quad + \frac{\mu}{2} [H(I, J, n)] \{ [X^{(t)}(n+1, J)] - [X^{(t-1)}(n+1, J)] \}, \end{aligned} \quad (49)$$

where $[E]$, $[L]$, and $[H]$ are square matrices which are functions of the harmonic number, n . Expressions for the elements of these matrices, which are based on quasi-static aerodynamics, are presented in Appendix II.

It would be expected that the increments in the n^{th} harmonic generalized aerodynamic forces, $[\Delta^{(t)}G(n, I)]$, would be primarily caused by the changes in the n^{th} harmonic blade motions and, thus, to be given by the first term on the right-hand side of Equation (49). The $[L]$ and $[H]$ matrix terms give the coupling of $\Delta^{(t)}[G(n, I)]$ with variables of harmonic number one below and one above the harmonic number of the generalized forces under consideration. Couplings of this type would be expected to be of first order in the advance ratio, μ . Couplings with harmonic variables having greater separations in harmonic number (i. e., those in the matrices $[X(n+2, J)]$, $[X(n-2, J)]$, etc.) would be expected to be of second or higher order in the advance ratio and are not included in estimating $\Delta^{(t)}[G(n, I)]$. It will be noted that the $[L]$ and $[H]$ matrices produce couplings between the generalized forces acting in symmetric modes and the motions in antisymmetric modes and vice versa.

After substituting Equation (49) into Equation (47), the following equation results:

$$[F(I, J, n)][X^{(t)}(n, J)] = [Y^{(t)}(n, I)], \quad (50)$$

where

$$[F(I, J, n)] = [D(I, J, n)] + [E(I, J, n)], \quad (51)$$

$$\begin{aligned} [Y^{(t)}(n, I)] &= \frac{I}{\Omega^2} [G^{(t-1)}(n, I)] + [E(I, J, n)] [X^{(t-1)}(n, J)] + \frac{I}{\Omega^2} [Z(n, I)] + \frac{I}{\Omega^2} [Y_P(n, I)] \\ &\quad + \frac{\mu}{2} [L(I, J, n)] \Delta^{(t)} [X(n-1, J)] + \frac{\mu}{2} [H(I, J, n)] \Delta^{(t)} [X(n+1, J)], \end{aligned} \quad (52)$$

$$\left. \begin{aligned} \Delta^{(t)}[X(n-1, J)] &= [X^{(t)}(n-1, J)] - [X^{(t-1)}(n-1, J)] \\ \Delta^{(t)}[X(n+1, J)] &= [X^{(t)}(n+1, J)] - [X^{(t-1)}(n+1, J)] \end{aligned} \right\}. \quad (53)$$

The equations obtained by setting $n = 0, 1, \dots, 12$ in Equation (50) are all coupled together through the $[L]$ and $[H]$ matrix terms, giving a total of 208 individual simultaneous equations involving the 208 variables which are the elements in the $[X(n, J)]$ matrices with harmonic numbers ranging from 0 to 12. Although these are linear equations when the $[G]$ matrices are considered to be known quantities, it is impracticable to obtain a solution for them by matrix inversion because of the large number of variables involved. Consequently, another inner loop iterative solution is resorted to in the computational procedure.

The computation of the t^{th} approximation for the column matrices of harmonic variables starts by computing the $[Y_D^{(t)}]$ matrices which are the $[Y^{(t)}]$ matrices of Equation (52) neglecting the $[L]$ and $[H]$ matrix terms. This decouples the equations given by Equation (50) for different n 's and makes possible a solution of each matrix equation by inverting a 16×16 $[F]$ matrix,

$$[X^{(t)}] = [F^{-1}] [Y_D^{(t)}]. \quad (54)$$

The prime on the superscript in $[X^{(t)}]$ indicates a matrix obtained at an intermediate step in the iterative solution of Equation (50). Using the $[X^{(t)}]$ matrices obtained from Equation (54), the $\Delta^{(t)}[X]$ matrices in Equation (53) can be evaluated. It is then possible to use Equation (52) to make a second approximation for the $[Y^{(t)}]$ matrices including the $[L]$ and $[H]$ matrix terms. This inner loop iteration process can be repeated a specified number of times (denoted by $LGCD$) in order to obtain a satisfactory solution of Equation (50).

Once the $[X^{(t)}]$ matrices have been obtained, the next approximation for the generalized aerodynamic forces can be computed. Figure 13 is a schematic diagram of the complete computational procedure showing how the inner loop iterative solutions are used in the overall solution for the harmonic motions, required pitch angles and residual root shears. The overall process is repeated until the percentage variations in the generalized coordinates from one overall iteration to the next are below prescribed values.

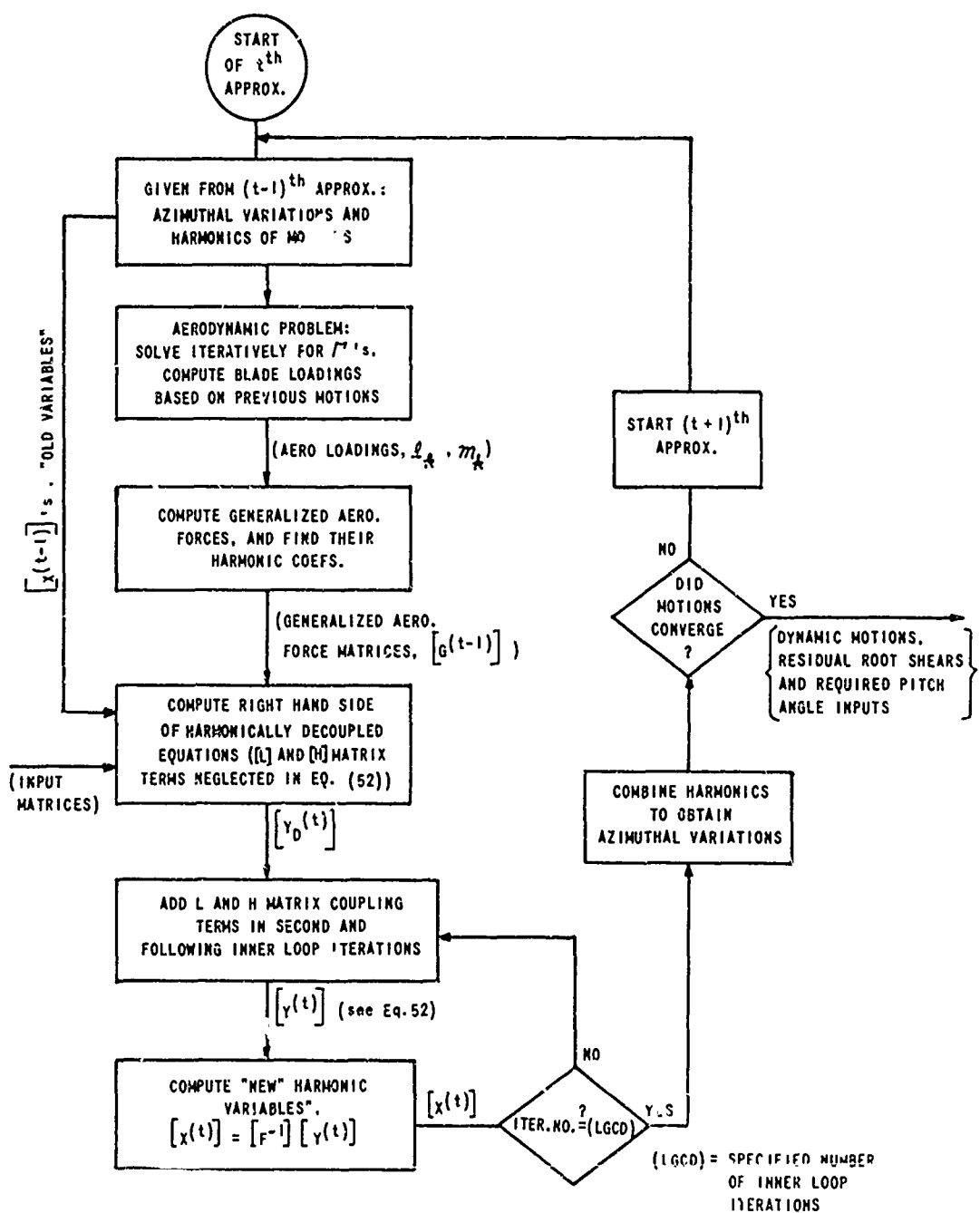


Figure 13 SCHEMATIC DIAGRAM OF PRINCIPAL STEPS IN ITERATIVE SOLUTION

4. RESULTS OF COMPUTATIONS FOR PITCH ANGLE INPUTS REQUIRED TO ELIMINATE NONCANCELING OSCILLATORY ROOT SHEARS

COMPUTATIONS FOR CONVENTIONAL PITCH CONTROL (WITH AND WITHOUT BLADE TORSION)

Flight condition DN67A with conventional collective and cyclic pitch controls is used as a reference case, and computations for this case were carried out to compare with results obtained using more complicated control inputs. Two sets of computations were made: one including deflections in the torsional modes indicated on Figure 11 (i. e., θ_1 , θ_2 , θ_3 , and θ_4) and the other setting these torsional deflections equal to zero.

The cyclic and collective pitch angles found in these solutions are presented in Table III and are the ones required to give the prescribed thrust per blade and tip-path-plane position for this flight condition (see Table I). Plots for the two cases were superimposed, which showed the azimuthal variations of the lift loadings and bending moments at eight radial stations along the span. These comparisons of results are not presented, since almost identical curves were obtained when torsional deflections were included or set equal to zero.

The noncanceling and canceling root shears obtained in these computer runs are shown in Table IV. Here, again, it is found that blade torsional deflections do not have a large effect upon the results when only zero harmonic collective and first harmonic cyclic control inputs are used. The differences in the amplitudes of the harmonic shears computed with and without blade torsion included are of the order of 10 percent of the average amplitudes or smaller.

Convergence difficulties in the computations, which were associated with torsional deflections, will be discussed later. These difficulties were overcome in computer run B-6, and the torsional deflections for this case were found to be small. In the first symmetric torsional mode, they were $|\theta_2| = 0.813, 0.164, 0.042$, and 0.043 degrees at $n = 0, 2, 4$, and 6 , respectively; while in the first antisymmetric torsional mode, they were $|\theta_1| = 0.294, 0.042, 0.048$, and 0.020 degrees at $n = 1, 3, 5$, and 7 , respectively. Torsional deflections in the second symmetric and antisymmetric torsional modes were an order of magnitude smaller.

It should be pointed out that, in the calculations made including torsion, the blade pitching and elastic axes were assumed coincident and the blade was assumed mass balanced about the elastic axis. If the blade had not been assumed to be mass balanced, the torsional degrees of freedom would probably have had a larger influence on the results.

Table III
EFFECT OF BLADE TORSION ON REQUIRED
COLLECTIVE AND CYCLIC PITCH ANGLES
FLIGHT CONDITION DN67A WITH CONVENTIONAL CONTROL

COMPUTER RUN	B-10	B-6
	NO BLADE TORSION	INCLUDING TORSIONAL MODES
($A_0 C_2$) COLLECTIVE	18.62 deg	19.27 deg
($A_1 C_1$) CYCLIC - COS COMP.	3.56 deg	3.26 deg
($B_1 C_1$) CYCLIC - SIN COMP.	-5.34 deg	-5.36 deg
CYCLIC, TOTAL AMPLITUDE	6.42 deg	6.27 deg
CYCLIC, PHASE ANGLE	56.30 deg	58.70 deg

Table IV
EFFECT OF BLADE TORSION ON HARMONIC ROOT SHEARS
FLIGHT CONDITION DN67A WITH CONVENTIONAL CONTROL

COMPUTER RUN B-10		COMPUTER RUN B-6		
NO BLADE TORSION		INCLUDING TORSIONAL MODES		
n	HARMONIC ROOT SHEARS (ONE BLADE) *			
	AMPLITUDE 1b	PHASE ANGLE (degrees)	AMPLITUDE 1b	PHASE ANGLE (degrees)
0	3200.0	0	3200.0	0
1	2731.0	-109.1	2749.0	-109.2
2	211.8	170.4	231.1	169.7
3	253.3	150.1	236.5	150.9
4	45.5	65.4	45.2	67.0
5	89.5	-43.4	96.9	-38.4
6	5.0	-141.9	6.7	-122.6
7	7.6	43.5	6.5	32.7
8	10.8	128.3	9.7	135.6
9	2.0	-64.9	2.1	-36.4
10	6.9	-31.6	10.0	-33.6
11	2.5	115.7	2.6	129.5
12	1.2	-179.9	1.1	-180.0

*ROOT SHEARS ARE NONCANCELING FOR $n = 0$ OR $n = \text{even}$
AND ARE CANCELING FOR $n = \text{odd}$

NOTE: AZIMUTHAL VARIATION OF n th HARMONIC ROOT SHEAR
= (Ampl.) $\times \cos(n\psi + \text{Phase Angle})$

ELIMINATION OF NONCANCELING ROOT SHEARS FOR FLIGHT CONDITION DN67A (BLADE TORSIONAL DEFLECTIONS ASSUMED ZERO)

In this section, the results of computations are discussed which were made to find the requirements for eliminating noncanceling root shears. The flexural motions of the blade were represented by the first two symmetric and first two antisymmetric bending modes, but it was assumed that there were no deflections in the torsional modes. Only the first symmetric and antisymmetric pitch modes (c_2 and c_1) were included, and deflections in the differential pitch control modes (c_3 and c_4) were set equal to zero.

As mentioned previously, there are four constraint equations introduced in the set of equations for each harmonic number n (see Equations (36) and (37)), and four of the harmonic variables for each n can be given prescribed values. The procedure used for making the torsional deflections zero was equivalent to assuming an infinite torsional stiffness and did not involve the constraint equations. Two of the constraint equations at each n were used to make all the harmonics of c_3 and c_4 equal to zero.

At $n = 1$, the remaining two prescribed variables are the cosine and sine components of the teetering motion which are necessary to establish the desired tip-path-plane position. At all higher odd harmonics, the sine and cosine components of the inputs in the first antisymmetric control modes are prescribed to be zero:

$$\left. \begin{array}{l} (A_n c_1) = 0 \\ (\beta_n c_1) = 0 \end{array} \right\} \quad n = 3, 5, 7, 9, 11.$$

The steady component of the root shear is prescribed to be equal to the desired thrust load per blade of 3200 pounds. The constraints used for a higher harmonic with n even are either that the harmonic coefficients of the root shears or the harmonic coefficients of the first control mode are to be zero. That is,

$$\left. \begin{array}{l} (A_n s_N) = 0 \\ (\beta_n s_N) = 0 \\ \text{or} \\ (A_n c_2) = 0 \\ (\beta_n c_2) = 0 \end{array} \right\} \quad n = 2, 4, 6, 8, 10, 12.$$

Table V presents data on the harmonic pitch angle inputs required to eliminate noncanceling root shears. The first two columns repeat the data given previously for the case of conventional pitch control. In computer run B-12, noncanceling harmonic shears were eliminated at the second and fourth harmonics by applying second and fourth

Table V
REQUIRED PITCH ANGLES TO ELIMINATE NONCANCELLING ROOT SHEARS
FLIGHT CONDITION DN67A (NO TORSIONAL DEFLECTIONS)

n	COMPUTER RUN B-10		COMPUTER RUN B-12		COMPUTER RUN B-8	
	PITCH ANGLES WITH CONVENTIONAL CONTROL		PITCH ANGLES TO ELIMINATE ROOT SHEARS AT n = 2,4		PITCH ANGLES TO ELIMINATE ROOT SHEARS ^T n = 2,4,6,8,10,12	
	AMPLITUDE (degrees)	PHASE ANGLE (degrees)	AMPLITUDE (degrees)	PHASE ANGLE (degrees)	AMPLITUDE (degrees)	PHASE ANGLE (degrees)
0	18.62	0	18.75	0	18.78	0
1	6.42	56.3	6.84	57.3	6.89	57.5
2			1.18	155.1	1.21	155.2
3			—	—	—	—
4			.63	41.7	.62	40.7
5					—	—
6					.15	-141.9
7					—	—
8					1.01	132.4
9					—	—
10					1.10	11.0
11					—	—
12					.25	-125.0

AZIMUTHAL VARIATION OF nth HARMONIC PITCH ANGLE = (Ampl.) x cos (nψ + Phase Angle)

Table VI
EFFECT OF HIGHER HARMONIC PITCH ANGLE INPUTS ON ROOT SHEARS
FLIGHT CONDITION DN67A (NO TORSIONAL DEFLECTIONS)

n	COMPUTER RUN B-10		COMPUTER RUN B-12		COMPUTER RUN B-8	
	CONVENTIONAL CONTROL		HIGHER HARMONIC CONTROL AT n = 2,4		HIGHER HARMONIC CONTROL AT n = 2,4,6,8,10,12	
	HARMONIC ROOT SHEARS (ONE BLADE) *					
n	AMPLITUDE (pounds)	PHASE ANGLE (degrees)	AMPLITUDE (pounds)	PHASE ANGLE (degrees)	AMPLITUDE (pounds)	PHASE ANGLE (degrees)
0	3200.0	0	3200.0	0	3200.0	0
1	2731.0	-109.1	2756.0	-109.1	2756.0	-109.1
2	211.8	179.4	0	0	0	0
3	253.3	150.1	72.5	144.6	75.1	154.6
4	45.5	65.4	0	0	0	0
5	89.5	-43.4	66.5	-48.2	77.7	-36.7
6	5.0	-141.9	5.3	-104.4	0	0
7	7.6	43.5	8.5	37.2	18.3	61.1
8	10.8	128.3	10.4	131.8	0	0
9	2.0	-64.9	1.5	-61.3	17.4	-66.0
10	8.9	-31.6	9.9	-25.3	0	0
11	2.5	115.7	2.0	101.1	11.4	145.3
12	1.2	-179.9	0.4	-1.9	0	0

*ROOT SHEARS ARE NONCANCELLING FOR n = 0 OR n = even AND ARE CANCELING FOR n = odd

AZIMUTHAL VARIATION OF nth HARMONIC ROOT SHEAR = (Ampl.) x cos (nψ + Phase Angle)

harmonic collective pitch control, while in computer run B-8, all noncanceling harmonic shears were eliminated through the twelfth harmonic by applying collective pitch control at all even harmonics through the twelfth. The root shears corresponding to these pitch inputs are given in Table VI and will be discussed later. Figure 14 presents a comparison of the pitch control schedules corresponding to the harmonic components given in Table V.

The pitch angle requirements for eliminating the second and fourth harmonic root shears are found to be approximately the same whether or not the noncanceling shears for the sixth through the twelfth harmonic are eliminated. Noncanceling shears can be eliminated at the sixth and twelfth harmonics with comparatively small pitch inputs. However, it is found that large collective pitch inputs are required at the eighth and tenth harmonics if the root shears at these harmonics are to be made zero. The presence of these large higher harmonic inputs results in a very irregular collective pitch schedule as shown by the curve for computer run B-8 on Figure 14.

A physical explanation of the need for the large higher harmonic pitch inputs is readily obtained by considering the effect of the dynamic response of the rotor. The aerodynamic forces due to pitch inputs not only produce root shears but also cause teetering and bending motions of the blade. At some harmonics, the inertia forces resulting from these teetering and bending motions can cause root shears which are nearly equal and opposite to the shears due to the aerodynamic forces. As a result, large pitch inputs may be required at some harmonics to bring about small changes in the corresponding root shears.

For example, when conventional control is assumed at flight condition DN67A, the eighth harmonic root shear due to aerodynamic forces has an amplitude of 29.2 pounds, while the total root shear, including dynamic effects, has an amplitude of 10.8 pounds. If an eighth harmonic pitch input is introduced to make the total eighth harmonic root shear zero, the contribution of the aerodynamic forces to the root shear is increased to an amplitude of 469.2 pounds. A compensating increase in the inertia forces occurs, making the resultant shear zero.

Thus, for this case, the eighth harmonic transmitted shear has been made zero only at the expense of introducing large eighth harmonic pitch inputs and large eighth harmonic aerodynamic and inertia force loadings. It is possible that this situation might be improved by the use of a different control mode such as differential rotation of the inner and outer sections of the blade which might change the relative magnitudes of the aerodynamic and inertia root shears. However, the results suggest that if the usual control mode is used which gives the same pitch inputs at all radial stations, it might be desirable to eliminate noncanceling root shears only through the fourth harmonic.

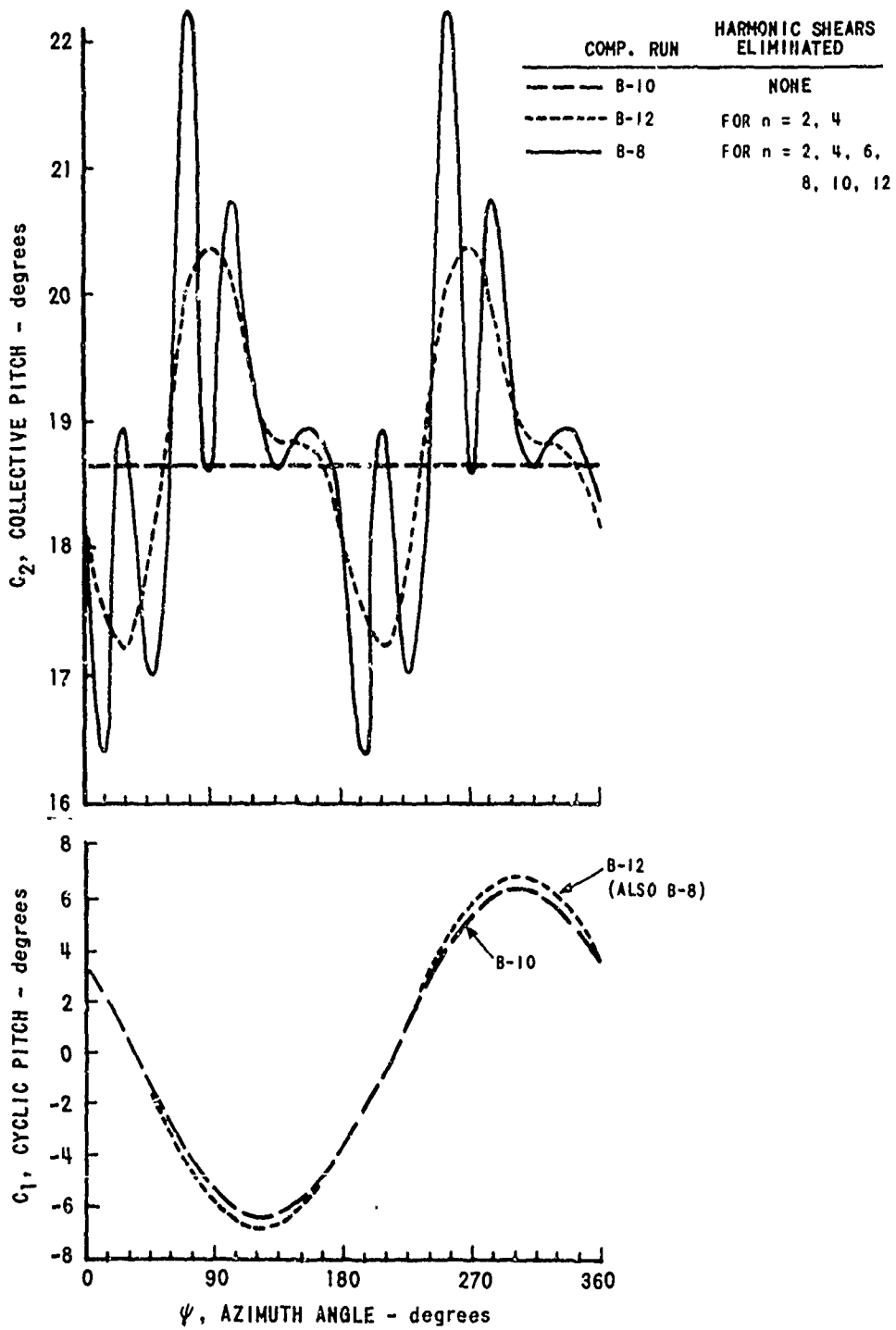


Figure 14 COMPARISON OF PITCH CONTROL SCHEDULES FOR ELIMINATING NONCANCELING HARMONIC ROOT SHEARS. FLIGHT CONDITION DN67A

In order to evaluate the penalties resulting from limiting the pitch angle inputs in this manner, the corresponding effects on the harmonics of the transmitted shears are shown in Table VI. It is found that the noncanceling shears at $n = 6, 8, 10$, and 12 , which were obtained for computer run B-12 (no pitch control at harmonics greater than $n = 4$), are essentially the same as those obtained in computer run B-10 (conventional control). The canceling root shears at the seventh, ninth and eleventh harmonics in computer run B-12 are also approximately of the same magnitude as those obtained with conventional control, but those for computer run B-8 are considerably higher. This result indicates that an appreciable interharmonic coupling exists through the aerodynamic forces.

The azimuthal variations of the noncanceling root shears corresponding to the harmonic data in Table VI are plotted on Figure 15.

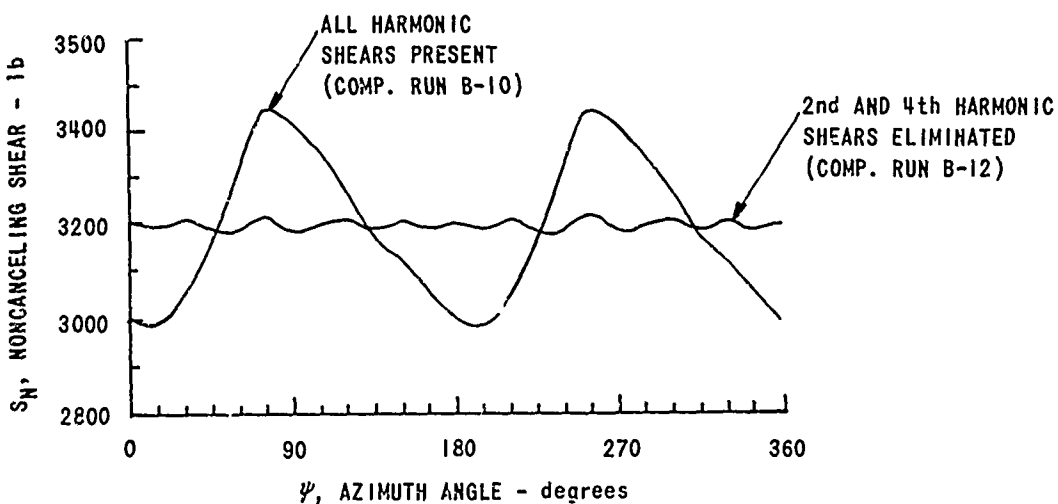


Figure 15 AZIMUTHAL VARIATION OF NONCANCELLING ROOT SHEARS.
FLIGHT CONDITION DN67A

Results are not shown for computer run B-8 in which all oscillatory noncanceling root shears were eliminated. The curve for this run would be a constant value of $S_N = 3200$ pounds and is not presented to avoid obscuring the other data. It can be seen that when pitch control is used to make the second and fourth harmonics of the root shear zero, the principal part of the oscillatory shear is eliminated.

Figures 16 and 17 show the effect of higher harmonic pitch control on the oscillatory lift loadings at several radial stations. The steady components of lift are not shown on these plots. On Figure 16, the results for computer run B-12 (pitch control to eliminate root shears at $n = 2, 4$) are compared with those for computer run B-10 (conventional control). On Figure 17, the results for computer run B-8 (all noncanceling root shears eliminated) are compared with the results for the case of conventional control.

It is apparent from Figures 16 and 17 that the elimination of harmonic root shears by pitch angle inputs in mode c_2 (i.e., equal angle changes at all radial stations) does not eliminate the azimuthal variation in the lift loadings. Large high-frequency variations in lift loadings, particularly near the blade tip, were obtained for the case in which all noncanceling harmonic shears were eliminated (see Figure 17). When only the second and fourth harmonic shears are eliminated, the magnitudes of the loadings do not, in general, get larger than those with conventional control (see Figure 16). However, the changes in the harmonic content due to higher harmonic control result in differences in the azimuthal variations of the loadings for the two cases.

Table VII presents the harmonics and maximum peak-to-peak amplitudes of the bending moments determined for the same conditions as considered in Figures 16 and 17. The most noticeable changes from the case of conventional control are large reductions in the second and third harmonic bending moments and a reduction in the peak-to-peak moments at the inboard stations. The bending moments from the eighth through the twelfth harmonic are, in general, larger for the case when all noncanceling shears are eliminated than in the case when only the second and fourth harmonic shears are eliminated, as would be expected from the lift loading curves. These moments would probably have been larger compared to the lower harmonic moments if additional bending modes had been included in the analysis which were closer to resonance with the exciting forces at the eighth and tenth harmonics.

ELIMINATION OF NONCANCELLING ROOT SHEARS. COMPARISON OF REQUIREMENTS FOR FLIGHT CONDITIONS DN66A, DN67A, AND DN68A

The results considered in the preceding section have all been obtained for the same basic flight condition, DN67A. Computations were also made to find the pitch angle inputs required to eliminate all noncanceling root shears for flight conditions DN66A and DN68A. The required pitch angles for the three flight conditions are compared in Table VIII. The differences in the required second and fourth harmonic pitch angle inputs are not large for the rpm difference of flight conditions DN67A and DN68A, but there are significant differences in the required inputs for the sixth to the tenth harmonic. Large differences in the required pitch angle inputs are found at all harmonics for the two conditions differing only in flight velocity.

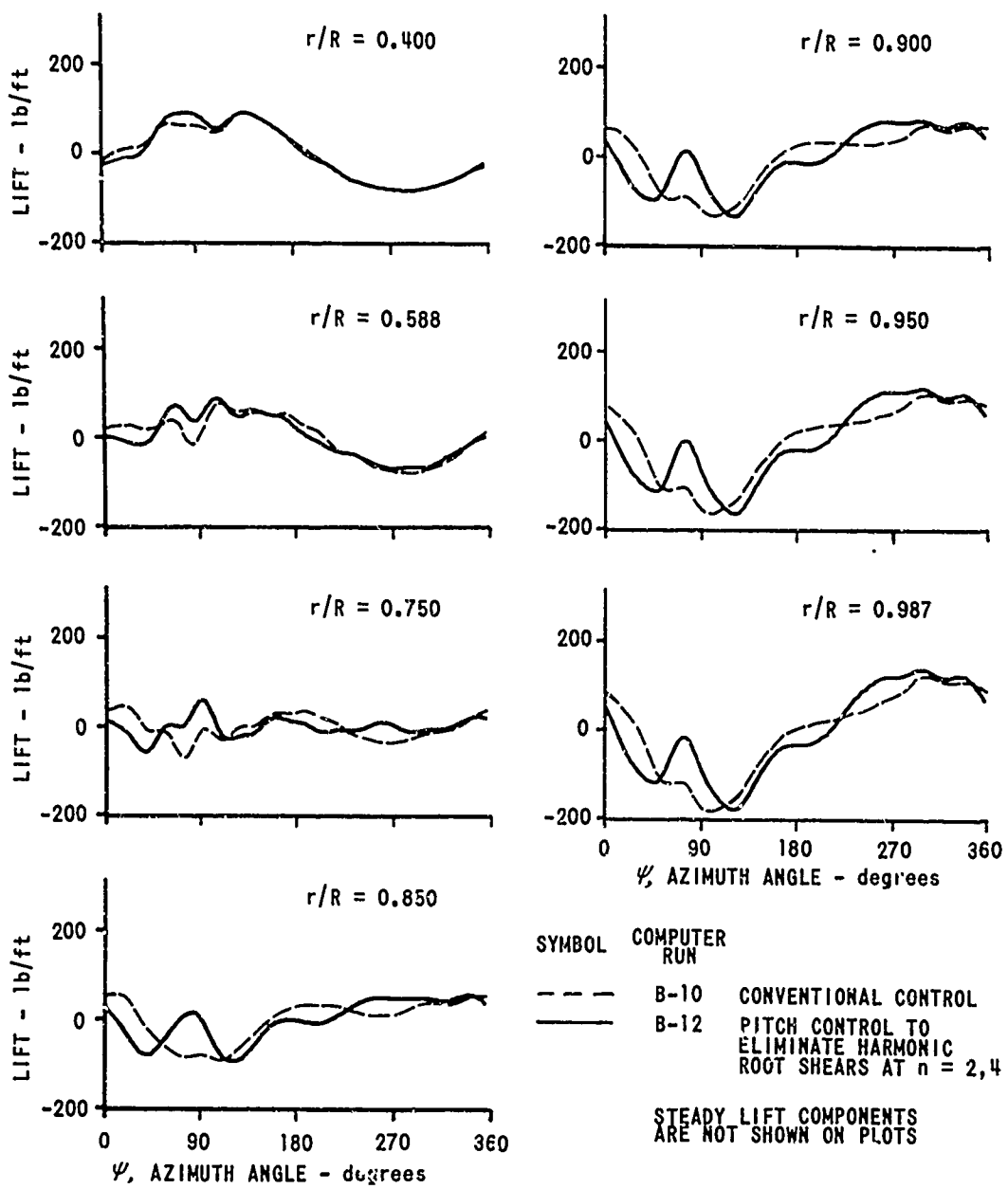


Figure 16 EFFECT OF HIGHER HARMONIC PITCH CONTROL ON OSCILLATORY LIFT LOADINGS. FLIGHT CONDITION DN67A. COMPUTER RUNS B-10 AND B-12

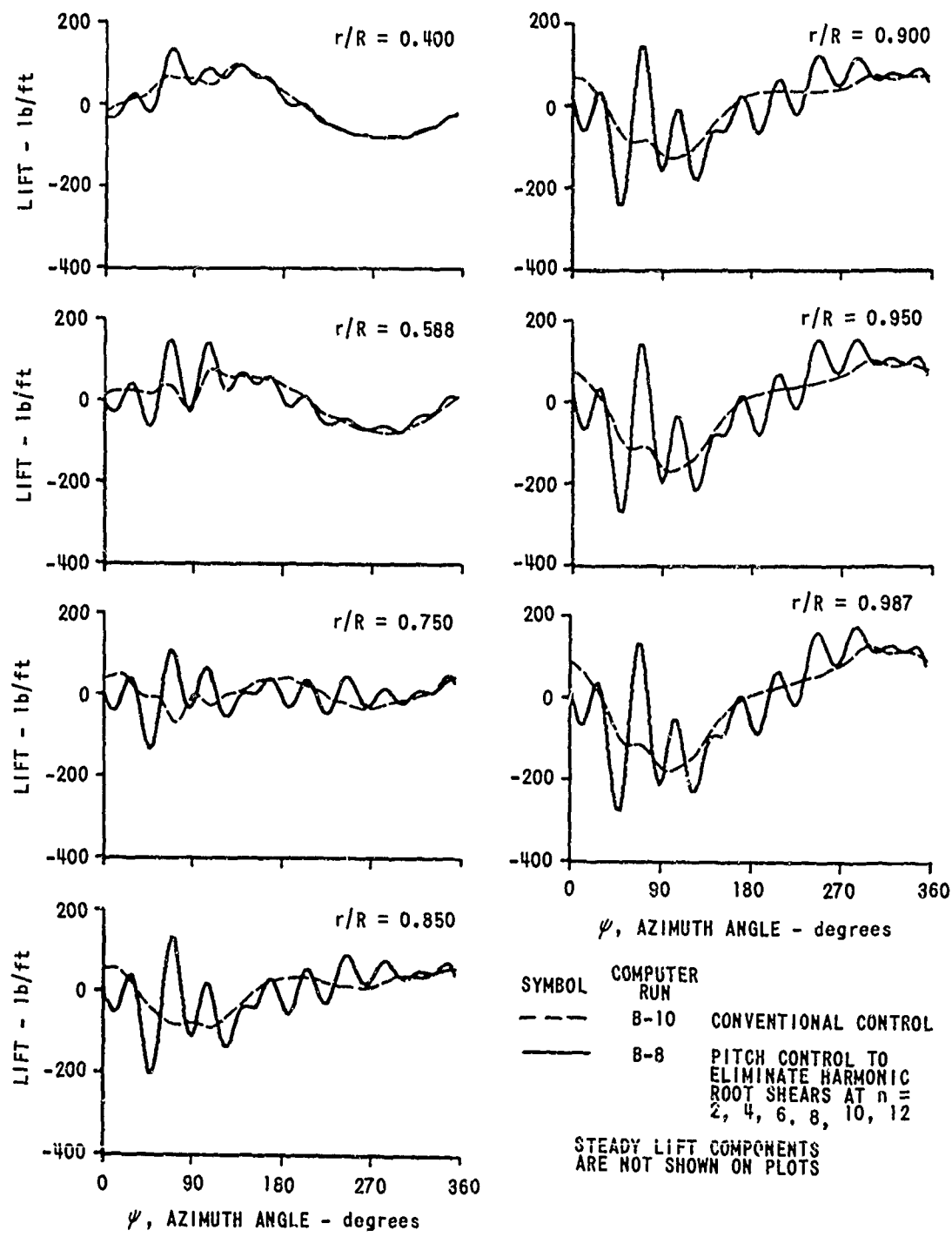


Figure 17 EFFECT OF HIGHER HARMONIC PITCH CONTROL ON OSCILLATORY LIFT LOADINGS. FLIGHT CONDITION DN67A. COMPUTER RUNS B-8 AND B-10

Table VII
HARMONIC AND PEAK-TO-PEAK AMPLITUDES OF BENDING MOMENTS
(FLIGHT CONDITION DN67A (NO TORSIONAL DEFLECTIONS))

COMPUTER RUN	B-10	B-12	B-8	B-10	B-12	B-8
BENDING MOM. (in.-lb) AT $r/R=0.15$	BENDING MOM. (in.-lb) AT $r/R=0.36$					
	HARMONICS AT WHICH ROOT SHEARS MADE ZERO:				HARMONICS AT WHICH ROOT SHEARS MADE ZERO:	
n	NONE	n = 2,4	n = 2,4,6,8,10,12	NONE	n = 2,4	n = 2,4,6,8,10,12
0	1775	1773	1831	1006	984	981
1	3141	3324	3287	2490	2628	2618
2	3549	627	695	469	157	160
3	1814	854	881	1273	517	523
4	430	621	615	69	83	69
5	1874	1619	1913	760	649	765
6	153	119	116	19	16	16
7	152	164	140	55	59	55
8	68	64	271	8.3	8.3	18
9	50	53	27	18	19	11
10	36	30	203	4.0	3.7	9.7
11	23	19	42	9.5	7.3	20
12	5	4	13	0.4	0.4	0.2
PEAK TO PEAK	15305	10010	10798	7973	6696	6948
BENDING MOM. (in.-lb) AT $r/R=0.60$	BENDING MOM. (in.-lb) AT $r/R=0.80$					
	HARMONICS AT WHICH ROOT SHEARS MADE ZERO:				HARMONICS AT WHICH ROOT SHEARS MADE ZERO:	
n	NONE	n = 2,4	n = 2,4,6,8,10,12	NONE	n = 2,4	n = 2,4,6,8,10,12
0	1924	1875	1858	1551	1511	1497
1	3444	3616	3646	2539	2657	2698
2	452	330	346	344	269	282
3	1413	476	471	913	361	373
4	226	224	180	187	185	149
5	593	541	646	1133	1007	1196
6	68	57	49	56	47	41
7	78	83	82	120	129	114
8	30	29	59	25	24	50
9	24	26	34	38	41	39
10	15	13	42	13	11	36
11	7.6	9.0	7.4	13	14	15
12	1.7	1.6	2.7	1.4	1.3	2.3
PEAK TO PEAK	7751	8286	8547	6210	7338	7635

Table VIII
 REQUIRED PITCH ANGLES TO ELIMINATE ALL
 NONCANCELLING ROOT SHEARS
 COMPARISON OF RESULTS FOR FLIGHT CONDITIONS DN66A, DN67A, AND DN68A

FLIGHT CONDITION	COMPUTER RUN D-2		COMPUTER RUN B-8		COMPUTER RUN C-2	
	DN66A V = 92.1 KNOTS Ω = 313 RPM		DN67A V = 111.4 KNOTS Ω = 313 RPM		DN68A V = 111.4 KNOTS Ω = 324 RPM	
<i>n</i>	PITCH ANGLE		PITCH ANGLE		PITCH ANGLE	
	AMPLITUDE (degrees)	PHASE ANGLE (degrees)	AMPLITUDE (degrees)	PHASE ANGLE (degrees)	AMPLITUDE (degrees)	PHASE ANGLE (degrees)
0	17.34	0	18.78	0	18.00	0
1	4.78	59.1	6.89	57.5	6.07	57.3
2	.57	161.3	1.21	55.2	1.06	153.8
3						
4	.24	8.4	.62	40.7	.65	39.8
5						
6	.64	-116.2	.15	-141.9	.30	-140.4
7						
8	.66	111.7	1.01	132.4	1.17	98.9
9						
10	1.94	4.4	1.10	11.0	.25	-5.0
11						
12	.80	-123.9	.25	-125.0	.21	-123.0

AZIMUTHAL VARIATION OF *n*th HARMONIC PITCH ANGLE = (Ampl.) $\times \cos(n\psi + \text{Phase Angle})$

CONVERGENCE DIFFICULTIES IN COMPUTER SOLUTION

In the first attempt to solve for the ordinary cyclic and collective pitch control inputs for trimmed flight (including the effects of bending and torsional deflections), the solution failed to converge. It was found that this difficulty resulted from the natural frequency of the first anti-symmetric torsional mode being very close to the frequency of the fifth harmonic exciting forces. Near this resonance, the inertia and spring forces are nearly balanced and the amplitude of the torsional response is largely determined by the effective aerodynamic damping forces. Under these conditions, the convergence of the computational solution is quite sensitive to the accuracy of the linearized aerodynamics used in predicting the variation in the generalized torsional force from one iteration to the next. By analyzing the data from the solution that did not converge, it was possible to make a better estimate of the aerodynamic coefficients for the torsional mode than was obtained from the quasi-static theory of Appendix II. When these revised coefficients were used in the computation, satisfactory convergence resulted.

Convergence difficulties were also encountered in some of the computations made with higher harmonic pitch control. The failure for convergence in these cases is believed to be due to the sensitivity of the solution to the estimated aerodynamic coefficients near resonant conditions arising from the coupling of the control modes with the torsional and bending modes. Computations were not carried out to determine if convergence could also be obtained in these cases by improving the estimates of the linearized aerodynamic coefficient in the $[E]$ matrix.

CONCLUSIONS AND RECOMMENDATIONS

The following specific conclusions are reached on the basis of this investigation:

1. The computations of the geometric angle of attack required to eliminate all oscillatory air loads show that the radial variations of the required angles are not the same for different flight conditions. Although some of the radial variations are fairly simple, a number of the radial plots of required angles on Figure 9 showed a pronounced "S" shape. Thus, it is concluded that it would be a difficult undertaking to design a pitch control system for the elimination of all oscillatory air loads.
2. It is found that the dynamic response of a rotor to higher harmonic pitch inputs has an important effect on the pitch angles required to eliminate oscillatory root shears.
3. All noncanceling vertical root shears of the teetering two-bladed rotor from the second through the twelfth harmonic can be eliminated with higher harmonic pitch angle control introduced at the blade root (as in conventional pitch control systems). The largest part of the oscillatory transmitted root shears can be removed by only using pitch angle inputs at the second and fourth harmonics.
4. The amplitudes and phase angles of the pitch inputs required to eliminate all noncanceling root shears change appreciably with flight condition.
5. It appears undesirable to attempt to eliminate all noncanceling harmonic root shears using a control system with pitch inputs introduced at the blade root. Higher harmonic pitch inputs, introduced to eliminate transmitted root shears, excite dynamic blade motions, and the inertia forces due to these motions also produce root shears. It is found at some harmonic numbers (depending upon the blade parameters and the flight condition) that the root shears due to these inertia forces are almost equal and opposite to the root shears due to the corresponding aerodynamic forces. This means that large pitch angle inputs and large blade dynamic motions may result from

trying to eliminate comparatively small root shears. It appears undesirable to introduce control inputs at harmonic numbers where such conditions exist.

The results of this study, which show that appropriate pitch angle inputs can produce significant reductions in the transmitted oscillatory root shears, offer definite encouragement for the application of this approach to reduce fuselage vibrations. However, a number of questions remain to be answered before it will be possible to establish the value and feasibility of using higher harmonic pitch control for this purpose. In particular, the following research is recommended for answering these questions:

1. Determine the influence of the pitch angle inputs which are introduced to remove oscillatory vertical forces on the oscillatory drag and side forces transmitted to the fuselage. (Some effort might be directed towards adjusting the pitch inputs in such a manner as to reduce these horizontal forces as well as the vertical forces. However, this might prove to be a more difficult problem because of the nonlinear variation of drag forces with angle of attack.)
2. Compute the blade root pitching moments on a rotor incorporating higher harmonic pitch control. Determine if the reacting moments from the different blades will cancel or whether they will tend to excite fuselage vibrations.
3. Determine how helicopter performance is affected by the higher harmonic pitch inputs which are introduced to eliminate transmitted shears.
4. Since it appears that there are large differences in the higher harmonic pitch angle inputs required at different flight conditions, it is recommended that a study be made of the application of a servo system for controlling the pitch inputs which would use measured transmitted shears as a feedback signal. (Initial study of the stability of the combined rotor dynamics-servo system could probably best be done by using linearized aerodynamics.)
5. All computations which have been made in this study have been for the case of control inputs applied at the blade root in the symmetric or collective mode (c_z) and in the antisymmetric or cyclic mode (c_x). However, other modes of pitch input can be introduced in the computational procedure which has been

developed (e.g., symmetric differential motions of the inner and outer sections of the blade (c_4) or antisymmetric differential motions (c_3). It is recommended that the application of pitch modes c_3 and c_4 be studied, particularly at those harmonic numbers where inputs in the usual pitch modes (c_1 and c_2) tend to excite large dynamic responses.

6. Finally, it is recommended that a study be made of means of avoiding the convergence difficulties in the computation procedure which have been encountered at resonant conditions.

REFERENCES

1. Kelley, B., Helicopter Vibration Isolation, SAE Preprint, January 1948.
2. Smollen, L. E., Marshall, P., and Gabel, R., A Servo Controlled Rotor Vibration Isolation System for the Reduction of Helicopter Vibration, American Institute of Aeronautics and Astronautics IAS Preprint No. 62-34, January 1962.
3. Hooper, W. E., Ureka -- A Vibration Balancing Device for Helicopters, Journal of the American Helicopter Society, Vol. II, No. 1, January 1966.
4. Hirsch, H., Hutton, R. E., and Rasumoff, A., Effect of Spanwise and Chordwise Mass Distribution on Rotor Blade Cyclic Stresses, American Institute of Aeronautics and Astronautics IAS Preprint No. 637, January 1956.
5. Bell Helicopter Company, An Experimental Investigation of a Second Harmonic Feathering Device on the UH-1A Helicopter, TCREC Technical Report 62-109, U. S. Army Transportation Research Command*, Fort Eustis, Virginia, June 1963.
6. Piziali, R. A., Cornell Aeronautical Laboratory, Inc., A Method for Predicting the Aerodynamic Loads and Dynamic Response of Rotor Blades, USAAVLABS Technical Report 65-74, U. S. Army Aviation Materiel Laboratories, Fort Eustis, Virginia, January 1966.
7. Measurement of Dynamic Airloads on a Full-Scale Semirigid Rotor, Bell Helicopter Report No. 525-099-001, TCREC Technical Report 62-42, U. S. Army Transportation Research Command*, Fort Eustis, Virginia, December 1962.
8. Daughaday, H., DuWaldt, F., and Gates, C., Investigation of Helicopter Blade Flutter and Load Amplification Problems, Journal of the American Helicopter Society, Vol. 2, No. 3, July 1957.

*Changed to U. S. Army Aviation Materiel Laboratories in 1965.

9. Targoff, W. P., The Bending Vibrations of a Twisted Rotating Beam, WADC Technical Report 56-27, Wright Air Development Center, Wright-Patterson AFB, Ohio, December 1955.
10. DuWaldt, F. A., Gates, C. A., and Piziali, R. A., Cornell Aeronautical Laboratory, Inc., Investigation of the Flutter of a Model Helicopter Rotor Blade in Forward Flight, WADD Technical Report 60-479, Wright Air Development Division, Wright-Patterson AFB, Ohio, July 1960.

APPENDIX I
BLADE PARAMETERS USED IN COMPUTATIONS

GEOMETRIC PROPERTIES

The blade planforms considered in the computations are shown on Figure 5. A preconing angle of 3.0 degrees is used in all computations. In Section 4, a built-in twist (θ_B) is included which varies linearly from zero at $r = 23$ inches to -11.0 degrees at the blade tip.

NATURAL FREQUENCIES AND BENDING MODES

The natural bending frequencies and mode shapes for the rotating blade are based on computations using the associated matrix method of Reference 9, while the torsional frequencies were obtained using a Holzer-type computation. A summary is given in Table IX of the frequencies at the three flight conditions for which computations are carried out.

Table IX
 NATURAL BLADE FREQUENCIES USED IN COMPUTATIONS

	FLIGHT CONDITIONS DN66A AND DN67A		FLIGHT CONDITION DN68A	
	ω_{g_i} (rad/sec)	ω_{q_i}/Ω	ω_{g_i} (rad/sec)	ω_{q_i}/Ω
ω_{h_2} , FIRST SYMMETRICAL BENDING	38.8	1.18	40.0	1.18
ω_{h_4} , SECOND SYMMETRICAL BENDING	112.8	3.43	115.6	3.41
ω_{h_6} , THIRD SYMMETRICAL BENDING	-	-	-	-
ω_{θ_2} , FIRST SYMMETRICAL TORSION	168.8	5.14	169.2	5.00
ω_{θ_4} , SECOND SYMMETRICAL TORSION	440.9	13.40	441.5	13.01
ω_{h_3} , FIRST ANTISYMMETRICAL BENDING	96.4	2.94	99.2	2.93
ω_{h_5} , SECOND ANTISYMMETRICAL BENDING	171.6	5.23	175.6	5.18
ω_{θ_1} , FIRST ANTISYMMETRICAL TORSION	168.8	5.14	169.2	5.00
ω_{θ_3} , SECOND ANTISYMMETRICAL TORSION	440.9	13.40	441.5	13.01

Frequencies are given for the first and second symmetric and first and second antisymmetric bending and torsional modes. The frequency and mode shape of the third symmetric bending mode were not computed. The deflections in this mode were assumed to be zero in the numerical computations for the pitch angles required to eliminate root shears.

COEFFICIENTS IN EQUATIONS OF MOTION

The equations of motion as presented in Equations (34) and (35) of Section 3 are in a general form applicable to any blade. Expressions for the coefficients in these equations are readily obtained for specific configurations as done, for example, in Reference 8. The following assumptions which are made in the computations of Section 4 result in a number of the coefficients in the general equations becoming equal to zero.

1. The relatively small gyroscopic coupling terms are neglected.
2. The elastic and pitch axes are assumed to be coincident and to intersect with the shaft axis.
3. The blade is assumed to be mass balanced about the elastic axis.
4. It is assumed there is no elastic coupling between the bending and torsional modes.

For this case, the expressions for the mass, centrifugal force, and stiffness coefficients take the form

$$M_{h_i h_i} = \int_0^R f_{h_i}^2 m dr + \left[\left(\frac{df_{h_i}}{dr} \right)_{r=0} \right]^2 I_z \text{ (root fitting)}.$$

$$T_{h_i h_i} = - \int_0^R \left(\frac{df_{h_i}}{dr} \right)^2 \left[\int_r^R r m dr \right] dr + \left[\left(\frac{df_{h_i}}{dr} \right)_{r=0} \right]^2 I_z \text{ (root fitting)},$$

$$K_{h_i h_i} = \Omega^2 T_{h_i h_i} + \omega_{h_i}^2 M_{h_i h_i},$$

$$M_{\theta_i \theta_i} = \int_0^R \left(\frac{dI_x}{dr} + \frac{dI_z}{dr} \right) f_{\theta_i}^2 dr, \quad M_{\theta_i c_j} = \int_0^R \left(\frac{dI_x}{dr} + \frac{dI_z}{dr} \right) f_{\theta_i} f_{c_j} dr,$$

$$T_{\theta_i \theta_i} = \int_0^R \left(\frac{dI_z}{dr} - \frac{dI_x}{dr} \right) f_{\theta_i}^2 dr, \quad T_{\theta_i c_j} = \int_0^R \left(\frac{dI_z}{dr} - \frac{dI_x}{dr} \right) f_{\theta_i} f_{c_j} dr,$$

$$K_{\theta_i \theta_i} = \Omega^2 T_{\theta_i \theta_i} + \omega_{\theta_i}^2 M_{\theta_i \theta_i},$$

where m is the mass per foot, dI_x/dr is the moment of inertia per foot about the elastic axis due to the horizontal distribution of mass, and dI_z/dr is the moment of inertia per foot about the elastic axis due to the vertical distribution of mass. The vertical distribution of mass is neglected in treating the bending modes except for the contribution of the root fitting.

The numerical values of the nonzero coefficients which were used in the computations are summarized in Tables X and XI.

Table X
MASS, CENTRIFUGAL FORCE, AND STIFFNESS COEFFICIENTS
FOR TEETERING AND BENDING MODES

	$M_{h_i h_i}$ (lb sec ² /ft)	$M_{h_{0A} h_i}$ ($i = \text{odd}$) $M_{h_{0S} h_i}$ ($i = \text{even}$) (lb sec ² /ft)	$T_{h_i h_i}$ (lb sec ² /ft)	$K_{h_i h_i}$ (lb/ft)
TEETERING (h_1)	1.972	+2.847	-1.972	0
1 st SYMMETRICAL BEND. (h_2)	1.553	2.248	-2.107	57.5
1 st ANISYMMETRICAL BEND. (h_3)	1.359	-0.891	-10.612	1143
2 nd SYMMETRICAL BEND. (h_4)	1.060	-0.780	-10.191	2450
2 nd ANISYMMETRICAL BEND. (h_5)	1.327	0.470	-27.579	9236

Table XI
MASS, CENTRIFUGAL FORCE, AND STIFFNESS COEFFICIENTS
FOR TORSION AND CONTROL MODES

	$M_{\theta_i \theta_i}$ (lb ft sec ²)	$T_{\theta_i \theta_i}$ (lb ft sec ²)	$K_{\theta_i \theta_i}$ (lb ft per rad)
1 st ANTISYMMETRICAL TORSION (θ_1)	0.2179	-0.2294	5961
1 st SYMMETRICAL TORSION (θ_2)	0.2179	-0.2294	5961
2 nd ANTISYMMETRICAL TORSION (θ_3)	0.2466	-1.646	45156
2 nd SYMMETRICAL TORSION (θ_4)	0.2466	-1.646	46156

$$M_{\theta_1 c_1} = 0.2965 \text{ lb ft sec}^2 \quad T_{\theta_1 c_1} = -0.2965 \text{ lb ft sec}^2$$

$$M_{\theta_2 c_2} = 0.2965 \quad T_{\theta_2 c_2} = -0.2965$$

$$M_{\theta_3 c_1} = -0.1373 \quad T_{\theta_3 c_1} = 0.1373$$

$$M_{\theta_4 c_2} = -0.1373 \quad T_{\theta_4 c_2} = 0.1373$$

The structural damping coefficient is assumed to be $\zeta = 0.03$ in all bending and torsional modes.

APPENDIX II
EXPRESSIONS FOR ELEMENTS IN [E], [L], AND [H] MATRICES

In estimating the increments in the generalized aerodynamic forces from one iteration to the next of the computational procedure, the following expressions are used for the quasi-static lift and pitching moment loadings:

$$L = 2\pi\rho b \left\{ \frac{C_L}{2\pi} \left(V_i^2 \alpha - V_i \dot{h}_i + \frac{b}{2} V_i \ddot{\alpha} \right) + \frac{b}{2} (V_i \dot{\alpha} - \ddot{h}_i) \right\} \quad (5)$$

$$m \text{ (about midchord)} = \pi\rho b^2 \left\{ V_i^2 \alpha - V_i \dot{h}_i - \frac{1}{8} b^2 \ddot{\alpha} \right\} \quad (56)$$

where V_i , α , $\dot{\alpha}$ and \ddot{h}_i are given by Equations (17), (42), (43), and (44), respectively. The incremental generalized forces due to these loadings are computed by a procedure similar to that used in Reference 10 and can be expressed in the form

$$\begin{aligned} \Delta^{(t)} G_{q_i} &= \sum_j \left\{ A_{q_i \ddot{q}_j} \Delta^{(t)} \ddot{q}_j + \Omega A_{q_i \dot{q}_j} \Delta^{(t)} \dot{q}_j + \Omega^2 A_{q_i q_j} \Delta^{(t)} q_j \right\} \\ &\quad + \mu \sum_j \left\{ (\Omega S_{q_i \dot{q}_j} \sin \psi) \Delta^{(t)} \dot{q}_j + (\Omega^2 C_{q_i q_j} \cos \psi + \Omega^2 S_{q_i q_j} \sin \psi) \Delta^{(t)} q_j \right\}, \end{aligned} \quad (57)$$

when terms proportional to μ^2 are dropped. The symbol $\Delta^{(t)}$ preceding the symbol for a given quantity is again used to denote the change in that quantity from the $(t-1)^{th}$ to the $(t)^{th}$ approximation of the iterative solution.

Only one-half of the modes of the two-bladed teetering rotor need be included in each of the summations in Equation (57) because the terms involving the other modes are zero from symmetry considerations. Terms which are independent of μ are grouped together in the first sum. The only q_j modes to be included in this group are those having the same symmetry as the q_i mode. Terms proportional to μ are put in the second sum. For this sum, the only q_j modes included are those having the opposite symmetry to q_i .

In the case of periodic motion, each variable in Equation (57) can be expressed in the form of Equation (30) leading to the following equations for the harmonic coefficients of $\Delta^{(t)} G_{q_i}$:

$$\begin{aligned} \frac{1}{\Omega^2} \Delta^{(t)} (A_n G_{q_i}) &= \sum_j \left\{ (-n^2 A_{q_i \ddot{q}_j} + A_{q_i q_j}) \Delta^{(t)} (A_n q_j) + (n A_{q_i \dot{q}_j}) \Delta^{(t)} (B_n q_j) \right\} \\ &+ \mu \sum_j \left\{ \left[\frac{1}{2} (n-1) S_{q_i \dot{q}_j} + \frac{1}{2} C_{q_i q_j} \right] \Delta^{(t)} (A_{n-1} q_j) + \left(-\frac{1}{2} S_{q_i q_j} \right) \Delta^{(t)} (B_{n-1} q_j) \right. \\ &\quad \left. + \left[-\frac{1}{2} (n+1) S_{q_i \dot{q}_j} + \frac{1}{2} C_{q_i q_j} \right] \Delta^{(t)} (A_{n+1} q_j) + \left(\frac{1}{2} S_{q_i q_j} \right) \Delta^{(t)} (B_{n+1} q_j) \right\} \quad (58) \end{aligned}$$

$$\begin{aligned} \frac{1}{\Omega^2} \Delta^{(t)} (B_n G_{q_i}) &= \sum_j \left\{ (n A_{q_i \dot{q}_j}) \Delta^{(t)} (A_n q_j) + (-n^2 A_{q_i \ddot{q}_j} + A_{q_i q_j}) \Delta^{(t)} (B_n q_j) \right\} \\ &+ \mu \sum_j \left\{ \left(\frac{1}{2} S_{q_i q_j} \right) \Delta^{(t)} (A_{n-1} q_j) + \left[\frac{1}{2} (n-1) S_{q_i \dot{q}_j} + \frac{1}{2} C_{q_i q_j} \right] \Delta^{(t)} (B_{n-1} q_j) \right. \\ &\quad \left. + \left(-\frac{1}{2} S_{q_i q_j} \right) \Delta^{(t)} (A_{n+1} q_j) + \left[-\frac{1}{2} (n+1) S_{q_i \dot{q}_j} + \frac{1}{2} C_{q_i q_j} \right] \Delta^{(t)} (B_{n+1} q_j) \right\} \quad (59) \end{aligned}$$

These equations are combined into the following matrix form for convenience in the computer solution:

$$\begin{aligned} \frac{1}{\Omega^2} \left[\Delta^{(t)} G(n, J) \right] &= - \left[E(I, J, n) \right] \left[\Delta^{(t)} X(n, J) \right] \\ &+ \frac{\mu}{2} \left[L(I, J, n) \right] \left[\Delta^{(t)} X(n-1, J) \right] + \frac{\mu}{2} \left[H(I, J, n) \right] \left[\Delta^{(t)} X(n+1, J) \right]. \quad (60) \end{aligned}$$

In this expression, $[X(n, J)]$ is the column matrix which lists the harmonic cosine and sine coefficients of the root shear and the generalized coordinates representing the blade motions. (The forms for even and odd n are given explicitly in Equations (36) and (37).) The matrices $[X(n-1, J)]$ and $[X(n+1, J)]$ correspond to the $(n-1)^{th}$ and $(n+1)^{th}$ harmonics.

The forms of the 16×16 $[E]$, $[L]$ and $[H]$ matrices are indicated below by writing the expressions for typical terms in the sub-matrices obtained by partitioning. In each matrix, the first and ninth columns are zero because the root shears do not appear in Equations (58) and (59). Also, the seventh, eighth, fifteenth and sixteenth rows are zero since the corresponding equations are constraint equations rather than an expression of the equilibrium of generalized forces in the control modes.

$$[E(I, J, n)] = \begin{bmatrix} & & & & & & & \\ & & & & & & & \\ & & [n^2 A_{q_i \ddot{q}_j} - A_{q_i \dot{q}_j}] & & & & [n A_{q_i \dot{q}_j}] & \\ & & 0 & & & & 0 & \\ & & [0] & & & & [0] & \\ & & & & & & & \\ & & & & & & & \\ & & [n A_{q_i \dot{q}_j}] & & & & [n^2 A_{q_i \ddot{q}_j} - A_{q_i \dot{q}_j}] & \\ & & 0 & & & & 0 & \\ & & [0] & & & & [0] & \\ & & & & & & & \end{bmatrix}$$

$$[L(I, J, n)] = \begin{array}{|c|c|} \hline & \\ \hline & 0 \left[(n-1) S_{q_i \dot{q}_j} + C_{q_i \dot{q}_j} \right] & -S_{q_i q_j} \\ \hline & [0] & [0] \\ \hline & \\ \hline 0 & S_{q_i \dot{q}_j} & (n-1) S_{q_i \dot{q}_j} + C_{q_i \dot{q}_j} \\ \hline & [0] & [0] \\ \hline \end{array}$$

$$[H(I, J, n)] = \begin{array}{|c|c|} \hline & \\ \hline & 0 \left[-(I+n) S_{q_i \dot{q}_j} + C_{q_i \dot{q}_j} \right] & S_{q_i q_j} \\ \hline & [0] & [0] \\ \hline & \\ \hline 0 & -S_{q_i q_j} & -(I+n) S_{q_i \dot{q}_j} + C_{q_i \dot{q}_j} \\ \hline & [0] & [0] \\ \hline \end{array}$$

Expressions are given below for the A , S and C coefficients in terms of the blade parameters. The A coefficients appear only in the $[E(I, J, n)]$ matrix and the two modes coupled by each of the terms must have the same symmetry. On the other hand, the S and C coefficients appear only in the $[L]$ and $[H]$ matrices and couple modes of opposite symmetry.

$$A_{h_i h_j} = -\pi \rho \int b^2 f_{h_i} f_{h_j} dr$$

$$A_{h_i \dot{\theta}_j} = \pi \rho \int b^2 e f_{h_i} f_{\dot{\theta}_j} dr$$

$$A_{h_i \ddot{c}_j} = \pi \rho \int b^2 e_o f_{h_i} f_{c_j} dr$$

$$A_{\dot{\theta}_i \dot{\theta}_j} = \pi \rho \int b^2 e f_{\dot{\theta}_i} f_{\dot{\theta}_j} dr$$

$$A_{\dot{\theta}_i \ddot{c}_j} = -\pi \rho \int b^2 \left(e^2 + \frac{b^2}{8} \right) f_{\dot{\theta}_i} f_{c_j} dr$$

$$A_{\ddot{c}_i \dot{\theta}_j} = -\pi \rho \int b^2 \left(ee_o + \frac{b^2}{8} \right) f_{\dot{\theta}_i} f_{c_j} dr$$

$$A_{h_i \dot{h}_j} = -\rho \int c_{\ell_\alpha} b r f_{h_i} f_{h_j} dr$$

$$A_{h_i \dot{\theta}_j} = 2\pi \rho \int b \left\{ \frac{c_{\ell_\alpha}}{2\pi} \left(\frac{b}{2} + e \right) + \frac{b}{2} \right\} r f_{h_i} f_{\dot{\theta}_j} dr$$

$$A_{h_i \ddot{c}_j} = 2\pi \rho \int b \left\{ \frac{c_{\ell_\alpha}}{2\pi} \left(\frac{b}{2} + e_o \right) + \frac{b}{2} \right\} r f_{h_i} f_{c_j} dr$$

$$A_{\dot{\theta}_i \dot{h}_j} = -2\pi \rho \int b \left(\frac{b}{2} - \frac{c_{\ell_\alpha}}{2\pi} e \right) r f_{\dot{\theta}_i} f_{h_j} dr$$

$$A_{\dot{\theta}_i \dot{\theta}_j} = -\rho \int c_{\ell_\alpha} e \left(\frac{b}{2} + e \right) b r f_{\dot{\theta}_i} f_{\dot{\theta}_j} dr$$

$$A_{\theta_i \dot{c}_j} = -2\pi\rho \int \left\{ \frac{c_{\ell_\alpha}}{2\pi} e \left(\frac{b}{2} + e_0 \right) - (e_0 - e) \frac{b}{2} \right\} b r f_{\theta_i} f_{c_j} dr$$

$$A_{h_i h_j} = 0$$

$$A_{h_i \theta_j} = \rho \int c_{\ell_\alpha} b r^2 f_{h_i} f_{\theta_j} dr$$

$$A_{h_i c_j} = \rho \int c_{\ell_\alpha} b r^2 f_{h_i} f_{c_j} dr$$

$$A_{\theta_i \theta_j} = 2\pi\rho \int b \left(\frac{b}{2} - \frac{c_{\ell_\alpha}}{2\pi} e \right) r^2 f_{\theta_i} f_{\theta_j} dr$$

$$A_{\theta_i c_j} = 2\pi\rho \int b \left(\frac{b}{2} - \frac{c_{\ell_\alpha}}{2\pi} e \right) r^2 f_{\theta_i} f_{c_j} dr$$

$$S_{h_i \dot{h}_j} = -\rho R \int c_{\ell_\alpha} b f_{h_i} f_{h_j} dr$$

$$S_{h_i \dot{\theta}_j} = 2\pi\rho R \int b \left\{ \frac{c_{\ell_\alpha}}{2\pi} \left(\frac{b}{2} + e \right) + \frac{b}{2} \right\} f_{h_i} f_{\theta_j} dr$$

$$S_{h_i \dot{c}_j} = 2\pi\rho R \int b \left\{ \frac{c_{\ell_\alpha}}{2\pi} \left(\frac{b}{2} + e_0 \right) + \frac{b}{2} \right\} f_{h_i} f_{c_j} dr$$

$$S_{\theta_i \dot{h}_j} = -2\pi\rho R \int b \left(\frac{b}{2} - \frac{c_{\ell_\alpha}}{2\pi} e \right) f_{\theta_i} f_{h_j} dr$$

$$S_{\theta_i \dot{\theta}_j} = -\rho R \int c_{\ell_\alpha} e \left(\frac{b}{2} + e \right) b f_{\theta_i} f_{\theta_j} dr$$

$$S_{\theta_i \dot{c}_j} = -2\pi\rho R \int \left\{ \frac{c_{\ell_\alpha}}{2\pi} e \left(\frac{b}{2} + e_0 \right) - (e_0 - e) \frac{b}{2} \right\} b f_{\theta_i} f_{c_j} dr$$

$$S_{h_i h_j} = 0$$

$$S_{h_i \theta_j} = 2\rho R \int c_{\ell_\alpha} b r f_{h_i} f_{\theta_j} dr$$

$$S_{h_i c_j} = 2\rho R \int c_{\ell_\alpha} b r f_{h_i} f_{c_j} dr$$

$$S_{\theta_i h_j} = 0$$

$$S_{\theta_i \theta_j} = 4\pi \rho R \int b \left(\frac{b}{2} - \frac{c_{\ell_\alpha}}{2\pi} e \right) r f_{\theta_i} f_{\theta_j} dr$$

$$S_{\theta_i c_j} = 4\pi \rho R \int b \left(\frac{b}{2} - \frac{c_{\ell_\alpha}}{2\pi} e \right) r f_{\theta_i} f_{c_j} dr$$

$$C_{h_i h_j} = -\rho R \int c_{\ell_\alpha} b r f_{h_i} \frac{df_{h_j}}{dr} dr$$

$$C_{h_i \theta_j} = 0$$

$$C_{h_i c_j} = 0$$

$$C_{\theta_i h_j} = -2\pi \rho R \int b \left(\frac{b}{2} - \frac{c_{\ell_\alpha}}{2\pi} e \right) r f_{\theta_i} \frac{df_{h_j}}{dr} dr$$

$$C_{\theta_i \theta_j} = 0$$

$$C_{\theta_i c_j} = 0$$

Unclassified

Security Classification

DOCUMENT CONTROL DATA - R&D

(Security classification of title, body of abstract and indexing annotation must be entered when the overall report is classified)

1 ORIGINATING ACTIVITY (Corporate author) Cornell Aeronautical Laboratory, Inc. Buffalo, New York		2a REPORT SECURITY CLASSIFICATION Unclassified 2b GROUP
3 REPORT TITLE Suppression of Transmitted Harmonic Rotor Loads by Blade Pitch Control		
4 DESCRIPTIVE NOTES (Type of report and inclusive dates) Final Technical Report		
5 AUTHOR(S) (Last name, first name, initial) Daughaday, Hamilton		
6 REPORT DATE November 1967	7a TOTAL NO OF PAGES 90	7b NO OF REFS 10
8a CONTRACT OR GRANT NO DA 44-177-AMC-299(T)	9a. ORIGINATOR'S REPORT NUMBER(S) USAAVLABS TR 67-14	
b. PROJECT NO Task 1F125901A14604	9b OTHER REPORT NO(S) (Any other numbers that may be assigned this report) BB-2117-S-1	
10 AVAILABILITY/LIMITATION NOTICES This document has been approved for public release and sale; its distribution is unlimited.		
11 SUPPLEMENTARY NOTES	12 SPONSORING MILITARY ACTIVITY U. S. Army Aviation Materiel Laboratories, Fort Eustis, Virginia	
13 ABSTRACT <p>A method is developed for computing the pitch angle inputs required to eliminate the transmission of harmonic vertical forces from a helicopter rotor to its driving shaft. The inertia and aerodynamic forces due to dynamic blade motions are taken into account in the computations. In finding the aerodynamic loads, a realistic model is used which represents the wake vorticity by a mesh of segmented vortex filaments.</p> <p>Results of computations for three flight conditions are presented for a rotor which is approximately the same as the UH-1A configuration except for assumed differences in pitch control.</p>		

DD FORM 1 JAN 64 1473

Unclassified

Security Classification

Unclassified

Security Classification

14. KEY WORDS	LINK A		LINK B		LINK C	
	ROLE	WT	ROLE	WT	ROLE	WT
Transmitted Harmonic Rotor Loads Higher Harmonic Pitch Control						
INSTRUCTIONS						
1. ORIGINATING ACTIVITY: Enter the name and address of the contractor, subcontractor, grantee, Department of Defense activity or other organization (<i>corporate author</i>) issuing the report.	10. AVAILABILITY/LIMITATION NOTICES: Enter any limitations on further dissemination of the report, other than those imposed by security classification, using standard statements such as:					
2a. REPORT SECURITY CLASSIFICATION: Enter the overall security classification of the report. Indicate whether "Restricted Data" is included. Marking is to be in accordance with appropriate security regulations.	(1) "Qualified requesters may obtain copies of this report from DDC."					
2b. GROUP: Automatic downgrading is specified in DoD Directive 5200.10 and Armed Forces Industrial Manual. Enter the group number. Also, when applicable, show that optional markings have been used for Group 3 and Group 4 as authorized.	(2) "Foreign announcement and dissemination of this report by DDC is not authorized."					
3. REPORT TITLE: Enter the complete report title in all capital letters. Titles in all cases should be unclassified. If a meaningful title cannot be selected without classification, show title classification in all capitals in parenthesis immediately following the title.	(3) "U. S. Government agencies may obtain copies of this report directly from DDC. Other qualified DDC users shall request through _____."					
4. DESCRIPTIVE NOTES: If appropriate, enter the type of report, e.g., interim, progress, summary, annual, or final. Give the inclusive dates when a specific reporting period is covered.	(4) "U. S. military agencies may obtain copies of this report directly from DDC. Other qualified users shall request through _____."					
5. AUTHOR(S): Enter the name(s) of author(s) as shown on or in the report. Enter last name, first name, middle initial. If military, show rank and branch of service. The name of the principal author is an absolute minimum requirement.	(5) "All distribution of this report is controlled. Qualified DDC users shall request through _____."					
6. REPORT DATE: Enter the date of the report as day, month, year, or month, year. If more than one date appears on the report, use date of publication.	If the report has been furnished to the Office of Technical Services, Department of Commerce, for sale to the public, indicate this fact and enter the price, if known.					
7a. TOTAL NUMBER OF PAGES: The total page count should follow normal pagination procedures, i.e., enter the number of pages containing information.	11. SUPPLEMENTARY NOTES. Use for additional explanatory notes.					
7b. NUMBER OF REFERENCES: Enter the total number of references cited in the report.	12. SPONSORING MILITARY ACTIVITY. Enter the name of the departmental project office or laboratory sponsoring (<i>paying for</i>) the research and development. Include address.					
8a. CONTRACT OR GRANT NUMBER: If appropriate, enter the applicable number of the contract or grant under which the report was written.	13. ABSTRACT. Enter an abstract giving a brief and factual summary of the document indicative of the report, even though it may also appear elsewhere in the body of the technical report. If additional space is required, a continuation sheet shall be attached.					
8b, 8c, & 8d. PROJECT NUMBER: Enter the appropriate military department identification, such as project number, subproject number, system number, task number, etc.	It is highly desirable that the abstract of classified reports be unclassified. Each paragraph of the abstract shall end with an indication of the military security classification of the information in the paragraph, represented as (TS), (S), (C), or (U)					
9a. ORIGINATOR'S REPORT NUMBER(S): Enter the official report number by which the document will be identified and controlled by the originating activity. This number must be unique to this report.	There is no limitation on the length of the abstract. However, the suggested length is from 150 to 225 words.					
9b. OTHER REPORT NUMBER(S): If the report has been assigned any other report numbers (<i>either by the originator or by the sponsor</i>), also enter this number(s).	14. KEY WORDS. Key words are technically meaningful terms or short phrases that characterize a report and may be used as index entries for cataloguing the report. Key words must be selected so that no security classification is required. Identifiers, such as equipment model designation, trade name, military project code name, geographic location, may be used as key words but will be followed by an indication of technical context. The assignment of links, rules, and weights is optional.					

Unclassified

Security Classification

97-29-67